We are IntechOpen, the world's leading publisher of Open Access books Built by scientists, for scientists

4,800
Open access books available

122,000
International authors and editors

135M
Downloads

Our authors are among the

154
Countries delivered to

TOP 1%
most cited scientists

12.2%
Contributors from top 500 universities

CLARIVATE ANALYTICS BOOK CITATION INDEX INDEXED

WEB OF SCIENCE™

Selection of our books indexed in the Book Citation Index in Web of Science™ Core Collection (BKCI)

Interested in publishing with us?
Contact book.department@intechopen.com

Numbers displayed above are based on latest data collected.
For more information visit www.intechopen.com

17

Fluid Dynamics in Microchannels

Jyh-tong Teng et al.*
Department of Mechanical Engineering
Chung Yuan Christian University, Chung-Li
Taiwan

1. Introduction

1.1 Need for microchannels research

In contrast to external flow, the internal flow is one for which the fluid is confined by a surface. Hence the boundary layer develops and eventually fills the channel. The internal flow configuration represents a convenient geometry for heating and cooling fluids used in chemical processing, environmental control, and energy conversion technologies [1].

In the last few decades, owing to the rapid developments in micro-electronics and biotechnologies, the applied research in micro-coolers, micro-biochips, micro-reactors, and micro-fuel cells have been expanding at a tremendous pace. Among these micro-fluidic systems, microchannels have been identified to be one of the essential elements to transport fluid within a miniature area. In addition to connecting different chemical chambers, microchannels are also used for reactant delivery, physical particle separation, fluidic control, chemical mixing, and computer chips cooling.

Generally speaking, the designs and the process controls of Micro-Electro-Mechanical-Systems (MEMS) and micro-fluidic systems involved the impact of geometrical configurations on the temperature, pressure, and velocity distributions of the fluid on the micrometer (10^{-6} m) scale (Table 1.1). Therefore, in order to fabricate such micro devices effectively, it is extremely important to understand the fundamental mechanisms involved in fluid flow and heat transfer characteristics in microchannels since their behavior affects the transport phenomena for the bulk of MEMS and micro-fluidic applications.

Overall, the published studies based on an extensive literature reviews include a variety of fluid types, microchannel cross-section configurations, flow rates, analytical techniques, and channel materials. The issues and related areas associated with the microchannels are summarized in the following table (Table 1.2).

*Jiann-Cherng Chu[1], Chao Liu[2], Tingting Xu[2], Yih-Fu Lien[1], Jin-Hung Cheng[1], Suyi Huang[2], Shiping Jin[2], Thanhtrung Dang[3], Chunping Zhang[2], Xiangfei Yu[2], Ming-Tsang Lee[4], and Ralph Greif[5]
[1]*Department of Mechanical Engineering, Chung Yuan Christian University, Chung-Li, Taiwan*
[2]*School of Energy and Power Engineering, Huazhong University of Science and Technology, Wuhan, China*
[3]*Department of Heat and Refrigeration Technology, Hochiminh City University of Technical Education, Hochiminh City, Vietnam*
[4]*Department of Mechanical Engineering, National Chung Hsing University, Taichung, Taiwan*
[5]*Department of Mechanical Engineering, University of California at Berkeley, CA, USA*

Definition	The range of channel dimension
Conventional channels	$D_c > 3$ mm
Minichannels	3 mm $\geqq D_c >$ 200 μm
Microchannels	200 μm $\geqq D_c >$10 μm
Transitional Microchannels	10 μm $\geqq D_c >$1 μm
Transitional Nanochannels	1 μm $\geqq D_c >$0.1 μm
Nanochannels	$D_c \leqq$0.1 μm

Table 1.1. Channel classification schemes [2]

General research areas	Related studies
1. **Cross-sections of microchannels** *-Triangle, Rectangle, Trapezoid, Circle, Square and Non-uniform.*	1. Size effect (Hydraulic diameter) 2. Aspect ratio 3. Entrance effect
2. **Materials of microchannels** *- Silicon, Nickel, Polycarbonate, Polyamide, Fused silica, Stainless steel, Copper, Aluminum, Brass, Glass, Oxidized silicon,* SiO_2, Polyvinylchloride, *Poly-dimethylsiloxane(PDMS), poly-methyl* methacrylate *(PMMA).*	1. Surface roughness 2. Contact angle 3. Hydrophilic and hydrophobic property 4. Electrical double layer (EDL) 5. Thermo-physical properties
3. Types of flows *-* N_2, H_2, *Ar, Water, R-134a, Methanol, Iso-propanol, Aqueous KCI, Fluorinert fluid FC-84, Vertrel XF, Air, Helium, Silicon oil.*	1. Polarity 2. Rarefaction effect 3. Compressibility 4. Temperature jump 5. Non-slip and Slip 6. Joule heating
4. Flow rates *- Reynolds number, Mach number*	1. Critical Reynolds number of the transition to turbulence 2. Viscous heating or Viscous dissipation 3. Mal-distribution
5. Analytical techniques for microchannel flows *- Numerical simulation* *- Experimental analysis*	1. Flow pattern and visualization 2. Velocity field 3. Temperature distribution 4. Friction factor 5. Nusselt number 6. Poiseuille number

Table 1.2. Summary of research areas and discussed issues related to fluid flow in microchannel [3]

1.2 Research methodology

As the field of micro-fluidic systems continues to grow, it is becoming increasingly important to understand the mechanisms and fundamental differences involved in micro-scale fluid flow.

To study the thermal and hydrodynamic characteristics of fluid flow in microchannels, this work used experimental measure and numerical simulation to investigate the behavior of flow and temperature fields in microchannels. In this chapter, each part of the study will be described separately as follows.

1.2.1 Experimental work

To carry out the experiments of the flow in microchannels, first and foremost, a fluid flowing and measurement system, together with microchannel structures should be properly designed and built up. In this study, the details of experimental procedure involving the manufacturing of test chip, construction of experimental system, and analysis of experimental uncertainties will be described in the following sections.

In this chapter, an experimental flow chart related to the experimental procedure is shown in Fig. 1.1.

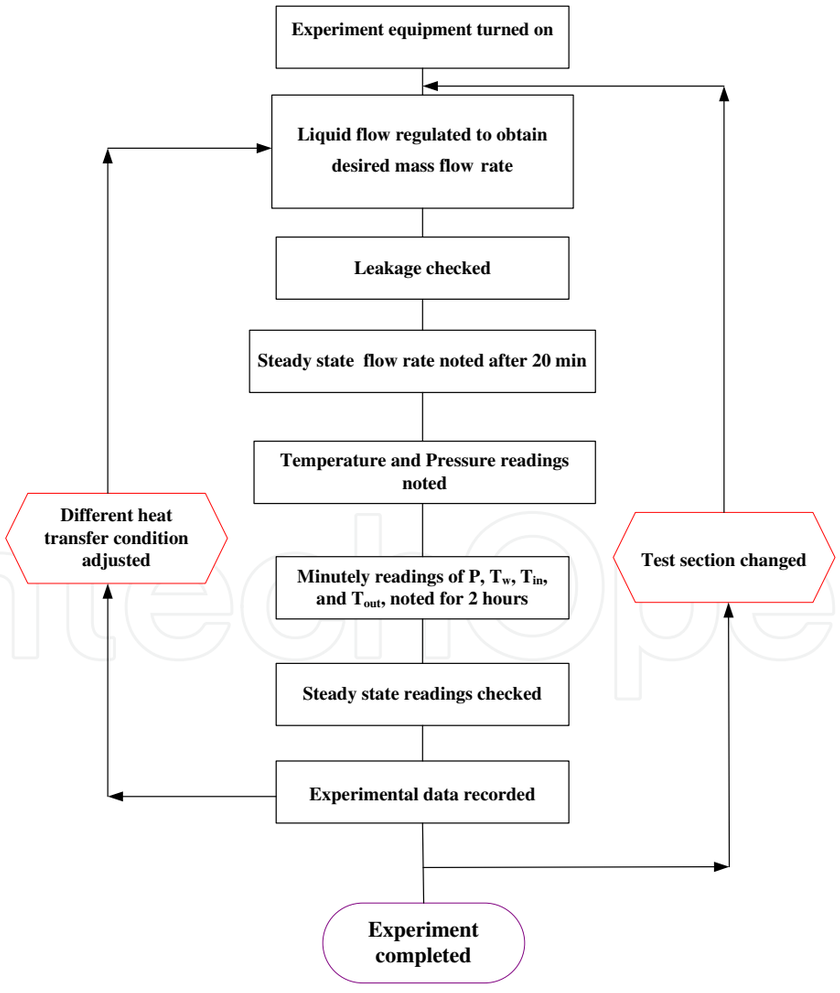

Fig. 1.1. Experimental flow chart [3].

1.2.2 Experimental system

The experimental system was divided into three parts – the test section, the water driving system, and the dynamic data acquisition section. In addition, DI water (deionized water) was used as the working fluid. The experimentally-measured data were composed of pressure drop through the microchannel, temperatures of DI water and substrate, and the mass flow rate. Each part of the experimental system will be described separately as follows:

1. Test section

Since measuring the local pressure and temperature along the flow path was difficult inside the microchannels, two sumps were machined in the PMMA block and were connected by microchannels with holes made by laser processing. A diaphragm type differential pressure transducer with ranges of 0-35 bars was connected to the sumps to measure the corresponding pressure drop across the inlet and outlet of the microchannel. Concerns had been raised that this kind of fitting could cause some dead volume resulting in the detection of false signals. However, to minimize the dead volume that might appear in the flow channel, extreme caution had been taken to ensure that no visible dead volume was observed there.

2. Water-driven system

Precision-controlled fluidic HPLC pump or injection pump was used to transport the DI water through the test section, and the flow rate was controlled in a range from 0.1 to 40 ml/min for the DI water flow. A filter (with a screening size of 0.2 μm) was installed midway to remove any possible particulates and contaminants that might be present in water under testing. For the case with heat generation, the stainless steel plate was electrically heated by directly connecting the bottom of test sections to a DC power supply that provided low voltage and high electric current. Once the working fluid was flowing into the test section, measurements of the pressure drop and temperature were done, followed by the weight measurement of the collected fluid using a precision electronic balance with an accuracy of 0.0001 g to obtain the mass flow rate of the system. In the meantime, the temperature of working fluid in the microchannel was measured by calibrated T-type Cu-Ni thermocouples to determine accurately the values of the water density and viscosity.

3. Dynamic data acquisition section

This section used an experimental platform with the test section laying horizontally on the platform, above which a digital microscope hooked with video capture card and signal cable to send the digital image to the PC for data-processing, ensuring that the working fluid passed through microchannel and that no left-over bubbles or impurities existed to block the flow channel that could lead to erroneous signals being obtained for the tests. In the meantime, a notebook PC and a network system were used to transmit data at a speed of one per 500 milliseconds. The data acquisition system for recording the electronic signals was implemented to obtain data from the differential pressure transducer and T-type thermocouples; the system was integrated through the instant monitoring software to record and analyze the data received. For each data point being measured, the flow was considered to be at a steady-state condition when the measured pressure drop and temperature remained unchanged for at least 10 minutes. Each case was repeated for at least three times to make sure that the arrangement could always produce reliable and reproducible results.

1.2.3 Numerical simulation

Numerical simulations were done by the CFD-ACE+ software [4] which provided an integrated numerical analysis of the continuity, momentum, and energy equations for the fluid flow and heat transfer. After specifying the boundary condition, CFD-ACE+ uses an iterative, segregated solution method where in the equation sets for variables such as pressure, velocity, and temperature are solved sequentially and repeatedly until a converged solution is obtained. In general, iterative equation solvers are preferred for this task because they are more economical in memory requirements than direct solvers. In CFD-ACE+ program, conjugate gradient solvers and algebraic multi-grid solver are provided to obtain the converged solution. In Chu et al. [3], the latter method was adopted. The basic idea of a multi-grid solution is to use a hierarchy of grids, from fine to coarse, to solve a set of equations, with each grid being particularly effective for removing errors of the wavelength characteristic of the mesh spacing on that grid.

In CFD-ACE+, the finite-volume approach is adopted due to its capability of conserving solution quantities. The solution domain is divided into a number of cells known as control volumes. In the finite volume approach of CFD-ACE+, the governing equations are made discrete and finite, and then numerically integrated over each of these computational cells or control volumes. An example of such a control volume is shown in Fig.1.2 [5].

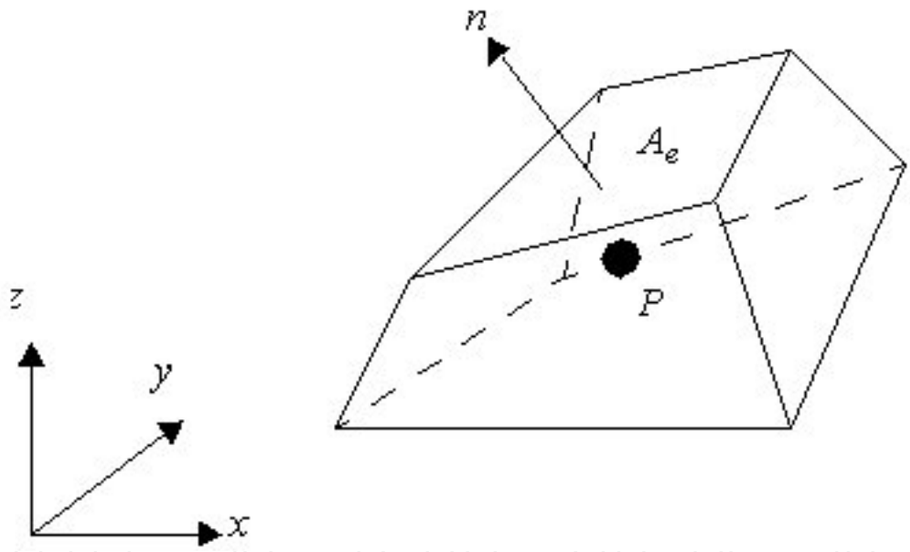

Fig. 1.2. 3D Computational Cell (Control Volume).

The geometric center of the control volume, which is denoted by *P*, is also often referred to as the cell center. CFD-ACE+ employs a co-located cell-centered variable arrangement, i. e., all dependent variables and material properties are stored at the cell center *P*. In other words, the average value of any quantity within a control volume is given by its value at the cell center.

Most of the governing equations can be expressed in the form of a generalized transport equation as shown in Eq. (1-1), which is also known as the generic conservation equation for a quantity Φ [5].

$$\underbrace{\partial(\rho\phi)/\partial t}_{\text{transient}} + \underbrace{\nabla\bullet(\rho\bar{V}\phi)}_{\text{convection}} = \underbrace{\nabla\bullet(\Gamma\nabla\phi)}_{\text{diffusion}} + \underbrace{S_\phi}_{\text{source}} \tag{1-1}$$

where S is the source term. The overall solution procedure in flowchart form for the solution algorithm is shown in Fig. 1.3. The number of iterations (NITER) can be defined to dictate how many times a procedure is repeated [6].

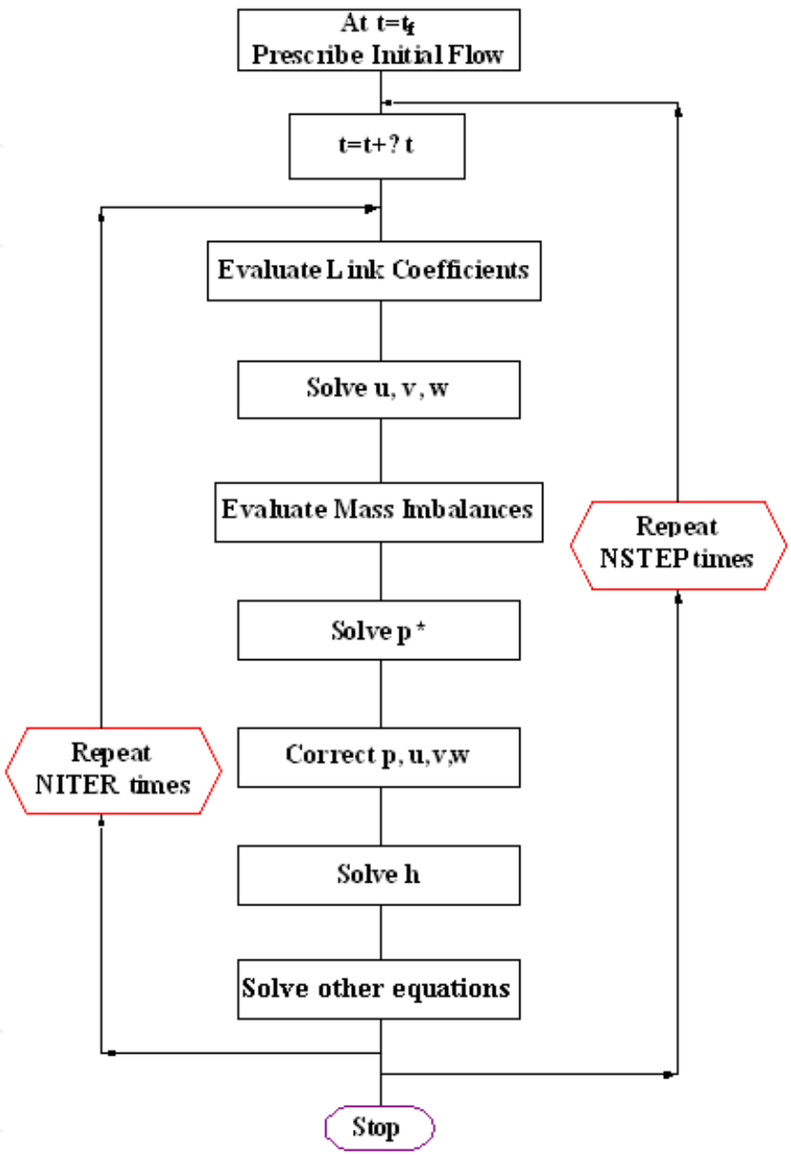

Fig. 1.3. Solution Flowchart.

2. Fundamental theory about flow motion

2.1 Pressure drop in single liquid-phase flow

2.1.1 Basic pressure drop correlations

For a non-circular cross section of the flow channels, the calculated hydraulic diameter D_h of a rectangular channel is computed by the following equation:

$$D_h = 4A_{ch}/P_w = 2WH/(W+H) \quad (2\text{-}1)$$

where A_{ch}, P_w, D_h, W and H represent as the areas of microchannel, wetted perimeter, hydraulic diameter, microchannel width and height, respectively.
The Reynolds number Re is defined as:

$$Re = \rho_m u_m D_h / \mu_m \tag{2-2}$$

where μ_m and ρ_m are mean dynamic viscosity and mean density of fluid at an arithmetic mean temperature ($T_m = (T_o+T_i)/2$), respectively. It should be noted that the fluid properties are functions of the temperature and values are obtained from correlations for dynamic viscosity (μ) correlations for dynamic viscosity (μ), thermal conductivity (k), specific heat (c_p), and density (ρ) of DI water.
Under actual conditions, the measured pressure drop includes the effect of the losses (1) in the bends and (2) at the entrance and exit, together with the frictional pressure drop in the microchannel. Phillips [7] suggested that the measured pressure drop was the sum of these components.

$$\Delta P_t = \frac{\rho u_m^2}{2}\left(K_c + K_e + 2(A_{ch}/A_p)^2 K_{90} + \frac{4 f_{app} L}{D_h} \right) \tag{2-3}$$

where ΔP_t, A_p, K_c, K_e, K_{90}, f_{app} and L are measured pressure drop, plenum area, contraction loss coefficient, expansion loss coefficient, bends loss coefficient and apparent friction factor, respectively. The loss coefficient K_{90} was recommended by Phillips [7]. K_c and K_e can be obtained from Kays and London [8]. According to the published investigations with regard to microchannels [9-12], these values of loss coefficient are usually obtained from the traditional relationships in macro-scale flow.
In addition, the method described above for determining minor losses was supported by the data obtained by Abdelall et al. [13], which showed that the experimentally measured loss coefficients associated with single-phase flow in abrupt area changes in microchannels were comparable to those obtained for large channels with the same area ratios.

2.1.2 Pressure drop in fully-developed laminar flow

For hydrodynamically fully developed flow, the velocity gradient at the channel wall can be readily calculated from the well-known Hagen-Poiseuille parabolic velocity profile for the fully developed laminar flow in a pipe. The Fanning friction factor f_c is expressed in the following form:

$$f_c = P_o / Re \tag{2-4}$$

where the Poiseuille number P_o is defined as P_o = fRe, the product of the friction factor and the Reynolds number.
For incompressible flow through horizontal channels of constant cross-sectional area, f_c can be calculated by Eq. (2-5), based on the mass flow rate and the pressure drop ΔP where the latter is due to the friction occurred inside the rectangular microchannel.

$$f_c = \frac{2\tau_w}{\rho_m u_m^2} = \frac{D_h \Delta P}{2\rho_m u_m^2 L} \tag{2-5}$$

where τ_w is the wall shear stress, L is the channel length, and u_m is the mean flow velocity.

A simple equation proposed by Shah and London [14] for fully developed, incompressible and laminar flow in a rectangular channel was used to predict the friction factor of straight rectangular microchannels. This equation, which has been used and proven to be adequate for predicting liquid flows in rectangular microchannels by several researchers [15-17], is expressed as follows:

$$f_c = 24(1 - 1.3553\alpha_c + 1.9467\alpha_c^2 - 1.7012\alpha_c^3 + 0.9564\alpha_c^4 - 0.2537\alpha_c^5) / \mathrm{Re} \quad (2\text{-}6)$$

Here f_c is the Fanning friction factor for a straight channel and α_c is the aspect ratio, which is the ratio of the dimension for the short side to that of the long side.

2.1.3 Pressure drop in developing laminar flow

The hydrodynamic entry length L_h for rectangular microchannels is given as follows [2].

$$L_h / D_h = 0.05Re \quad (2\text{-}7)$$

The apparent friction factor (f_{app}) includes the combined effects of frictional losses (pressure losses in developed region) and the additional losses in the developing region. The difference between the apparent friction factor (f_{app}) over a length x, measured from the entry location, and the fully developed Fanning friction factor (f_c) is expressed in terms of an incremental pressure defect K(x) as follows [3]:

$$\mathrm{K}(x) = \left(f_{app} - f_c\right)(4x) / \mathrm{D_h} \quad (2\text{-}8)$$

where K(x) is the Hagenbach factor in the above equation.

2.1.4 Fully developed and developing turbulent flow

Regarding fully developed turbulent flow in smooth microchannels, a number of correlations with comparable accuracies are available in the literatures. Blasius put forward the following equation which is used extensively nowadays.

$$f = 0.0791\mathrm{Re}^{-0.25} \quad (2\text{-}9)$$

Covering both the developing and developed flow regions, Phillips [18] used a more accurate equation for Fanning friction factor in a circular tube.

$$f = A\mathrm{Re}^B \quad (2\text{-}10)$$

where $A = 0.09290 + \dfrac{1.01612}{x / D_h}$ and $B = -0.26800 - \dfrac{0.32930}{x / D_h}$

For rectangular microchannels, Re is replaced with the laminar-equivalent Reynolds number given by

$$\mathrm{Re}^* = \frac{\rho u_m D_{le}}{\mu} = \frac{\rho u_m [(2/3) + (11/24)(1/\alpha_c)(2 - 1/\alpha_c)] D_{le}}{\mu} \quad (2\text{-}11)$$

where D_{le} is the laminar-equivalent diameter calculated by the term in the brackets.

2.1.5 Laminar-to-turbulent transition

The laminar-to-turbulent flow transition is another topic investigated by lots of researchers. In the entrance region of rectangular tubes with abrupt area change, the laminar-to-turbulent transition was reported to take place at a transition Reynolds number of R_{et} = 2200 for α_c =1 and at Ret = 2500 for parallel plates with α_c =0. For the other aspect ratios, a linear interpolation is recommended.

Some of the initial studies presented an early transition to turbulent flow in microchannels. However, several recent studies stated that the laminar-to-turbulent transition remained unchanged. For circular microtubes with diameter 171-520 μm, Bucci et al. [19] pointed that the transition occurred around R_{et} = 2000. The result of Baviere et al. [20] also indicated that the dimensions of smooth microchannels didn't affect the laminar-to-turbulent transition and the critical Reynolds number was still around 2300. It can be supported by a number of investigators, such as Schmitt and Kandlikar [21] for minichannels with $D_h < 1$ mm, and Li et al. [22] for 80 μm ≤ D_h ≤ 166.3 μm.

2.1.6 Pressure drop related to the change liquid properties

Eq. (2-6) provides the theoretical value of Fanning friction factor in rectangular microchannels at constant thermal properties of liquid suggested by Shah and London [23]. In the present experiments, the effect of liquid property variations cannot be neglected for a large temperature difference between inlet and outlet. Kays and London [8] suggested a corrected correlation for temperature dependent properties.

$$f / f_m = \left(\mu_w / \mu_m\right)^{\mathrm{M}} \tag{2-12}$$

where M = 0.58 for liquid heating, and M = 0.5 for liquid cooling; subscripts m and w are for the condition at the arithmetic mean fluid temperature and the condition at the wall temperature, respectively.

Then, the corrected form for the Shah and London correlation [23] according to the present study is

$$f_{\mathrm{c}}^{'} = f_{\mathrm{c}}\left(\mu_w / \mu_m\right)^{\mathrm{M}} \tag{2-13}$$

2.2 Basic heat transfer correlations in single liquid-phase flow

Results for the total heat transfer rate and the axial distribution of the mean temperature are derived as follows for the constant surface temperature condition (taking three heated walls in a channel for example, as shown in Fig. 2.1). Defining ΔT as $T_s - T_m$, the equation may be expressed as

$$\frac{dT_m}{dx} = -\frac{d(\Delta T)}{dx} = \frac{P_w}{\dot{m}c_p} h\Delta T \tag{2-14}$$

Separating variable and integrating from the tube inlet to the outlet yield

$$\int_{\Delta T_i}^{\Delta T_o} \frac{d(\Delta T)}{\Delta T} = -\int_0^L \frac{P_w}{\dot{m}c_p} h dx \tag{2-15}$$

or,

$$\ln(\frac{\Delta T_o}{\Delta T_i}) = -\frac{P_w L}{\dot{m} c_p}\left(\int_0^L \frac{1}{L} dx\right) \tag{2-16}$$

From the definition of the average convection heat transfer coefficient, it follows that

$$\ln(\frac{\Delta T_o}{\Delta T_i}) = -\frac{P_w L}{\dot{m} c_p}\bar{h}_L = -\frac{A_s}{\dot{m} c_p}\bar{h}_L, \qquad T_s = \text{constant} \tag{2-17}$$

where $\bar{h}_L$, or simply $\bar{h}$, is the average value of h for the entire channel, A_s is the heat exchange area between the working fluid and wall surface inside the channel. Rearranging,

$$\frac{\Delta T_o}{\Delta T_i} = \frac{T_s - T_{m,o}}{T_s - T_{m,i}} = \exp(-\frac{A_s}{\dot{m} c_p}\bar{h}), \qquad T_s = \text{constant} \tag{2-18}$$

For a general form of Eq. (2-18), one can obtain

$$\frac{T_s - T_m(x)}{T_s - T_{m,i}} = \exp(-\frac{P_w x}{\dot{m} c_p}\bar{h}), \qquad T_s = \text{constant} \tag{2-19}$$

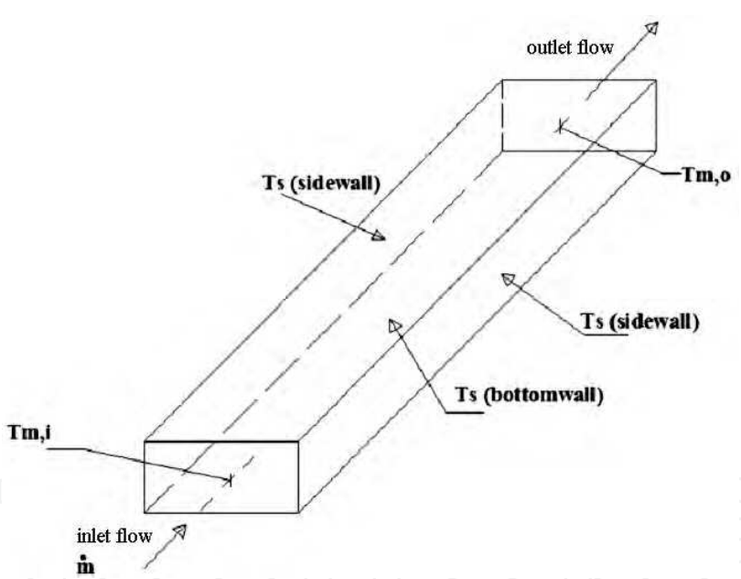

Fig. 2.1. Flow through a rectangular microchannel.

Since, by definition, Nusselt number equals to $h \cdot D_h/\lambda$, the average value of Nu for the entire channel can be expressed as

$$Nu = \frac{-D_h}{\lambda_m}\ln\left(\frac{\Delta T_o}{\Delta T_i}\right)\frac{\dot{m} c_p}{A_s}, \qquad T_s = \text{constant} \tag{2-20}$$

where λ_m and c_p are the mean thermal conductivity and heat capacity at constant pressure of DI water at an arithmetic mean temperature, respectively; A_s is the heat exchange areas between the walls and fluid.

For the heat exchange at the constant heat flux, the deduction of correlations can be found in [1]. Moreover, Lee et al. [24] examined the validity of conventional correlations and numerical analysis approaches in predicting the heat transfer behavior in microchannels for correctly matched inlet and boundary conditions.

3. Flow and heat transfer in microchannels of various configurations

3.1 Flow and heat transfer in V-shaped microchannels

A number of experimental and numerical investigations of single phase flow in microchannel have been extensively performed. However, most studies have experimental results obtained for microchannels with rectangular and circular cross-sections. The studies of thermo-fluidic characteristics in microchannels with a V-shaped cross-section are quite limited in this field. Thus, it is necessary to provide the present knowledge of V-shaped microchannel.

Flockhart and Dhariwal [25] measured the flow characteristics of distilled water inside trapezoidal microchannels with hydraulic diameters ranging from 50 to 120 μm and the Reynolds numbers below 600. They found that the flow characteristics of water in trapezoidal microchannels could be predicted by the numerical analysis based on the conventional theory.

Qu et al. [26, 27] used experimental and theoretical methods for the study of the thermo-fluidic characteristics of the trapezoidal microchannels with hydraulic diameters ranging from 62 to 169 μm. Results of their study indicated that the wall roughness of the microchannels might lead to lower Nusselt numbers as comparing with those obtained from the theoretical predictions. In addition, they also found that the experimentally determined friction factors in the trapezoidal microchannels were higher than those obtained from the conventional theory. They used a roughness-viscosity model developed by Mala and Li [16] to interpret the difference of friction factors obtained from the experimental data and those obtained from the conventional theory.

Hetsroni et al. [28] performed an experimental investigation of a microchannel heat sink for cooling of electronic devices. The heat sink had parallel triangular microchannels with a base of 250 μm. The results indicated that the temperature distribution at the exit of the triangular microchannel had a nonlinear distribution, and the instabilities caused fluctuations in the pressure drop and decrease in the heat transfer coefficient.

Wu and Cheng [29] conducted a series of experiments to measure the friction factor and convective heat transfer coefficient in trapezoidal silicon microchannels with different surface conditions. The results indicated that the geometric parameters had significant effect on the Nusselt number and Poiseuille number of trapezoidal microchannels, and the hydrophilic property at the surface of the microchannel enhanced the heat transfer capability of the trapezoidal silicon microchannels.

Wu and Cheng [30] experimentally studied the laminar flow of de-ionized water in smooth silicon microchannels of trapezoidal cross-sections with hydraulic diameters ranging from 25.9 to 291 μm. The measured results indicated that the Navier-Stokes equations were still valid for the laminar flow in the trapezoidal microchannel having a hydraulic diameter as small as 25.9 μm.

Tiselj et al. [31] performed the experimental and numerical analyses to evaluate the effect of axial heat flux on heat transfer in triangular microchannels with hydraulic diameter of 160 μm in the range of Reynolds numbers from 3.2 to 64. The experimental results revealed that

the temperature distribution of the triangular microchannels on the heated wall was in agreement with the numerical predictions obtained from conventional Navier-Stokes and energy equations.

Tiselj et al. [32] used three-dimensional numerical simulations for the study of the heat transfer characteristics of the fluid flowing through triangular microchannels. Their results indicated that a singular point existed near the exit of the channel. In addition, for the flow with higher Reynolds number, the singular point was closer to the exit of the channel.

Based on the conventional theory, Morin [33] developed a model to predict the viscous dissipation effects in a microchannel with an axially unchanging cross section. The microchannel geometries having rectangular, trapezoidal, and double trapezoidal were discussed in his work. The water and isopropanol were used as working fluids. The analytical results demonstrated that for different fluids the effect of viscous dissipation could play different roles and that the effect of viscous dissipation could become very significant for liquid flows when the hydraulic diameter was less than 100 μm. In addition, the rising temperature in an adiabatic microchannel could be expressed as a function of the Eckert number (defined as $Ec = u^2/c_v\Delta T$), Reynolds number, and Poiseuille number.

3.1.1 Model description

For the manufacture of V-shaped microchannels, photolithographic processes are particularly utilized for silicon wafers, and these processes initiated in the electronic field are well developed. When a photolithography-based process is employed, the microchannels having a cross-section fixed by the orientation of the silicon crystal planes can be fabricated; for example, the microchannels etched in <100> or in <110> silicon by using a potassium hydroxide (KOH) solution can form a V-shaped cross-section (as shown in Fig.3.1).

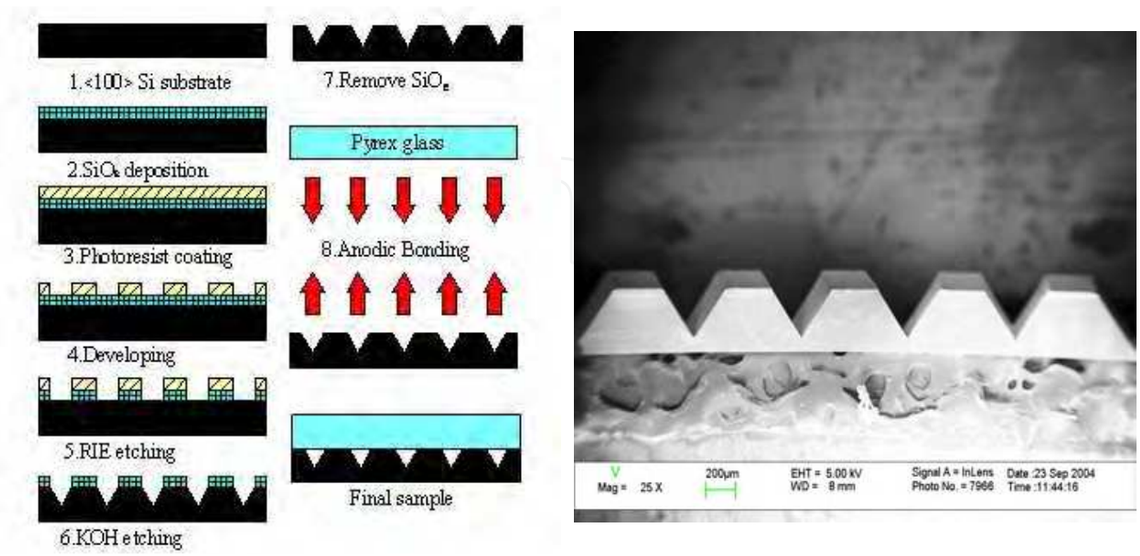

(a) (b)

Fig. 3.1. (a) Flowchart of micro-manufacture processing; (b) V-shaped microchannels.

3.1.2 Results and discussion

For incompressible, fully-developed laminar flow, the friction factor can be expressed in terms of the two experimentally obtained parameters – pressure drop and mass flow rate.

$$f_{exp} = \frac{D_h}{L}\left(\frac{2\Delta P_{exp}}{\rho V_{av}^{\ 2}} - \sum K_L\right) \tag{3-1}$$

where K_L is the friction factor for the minor loss. For the comparison of values of f vs. Re as shown in Fig. 3.2, the differences between the results obtained from numerical simulation and those from traditional correlation are within 2.5% of each other, within 6% between the numerical simulations and the experimental data, and with the f vs. Re values obtained from the experimental data and those obtained from the numerical simulations approaching a fixed value which is slightly lower than the value of 53.3 predicted by the traditional theory.

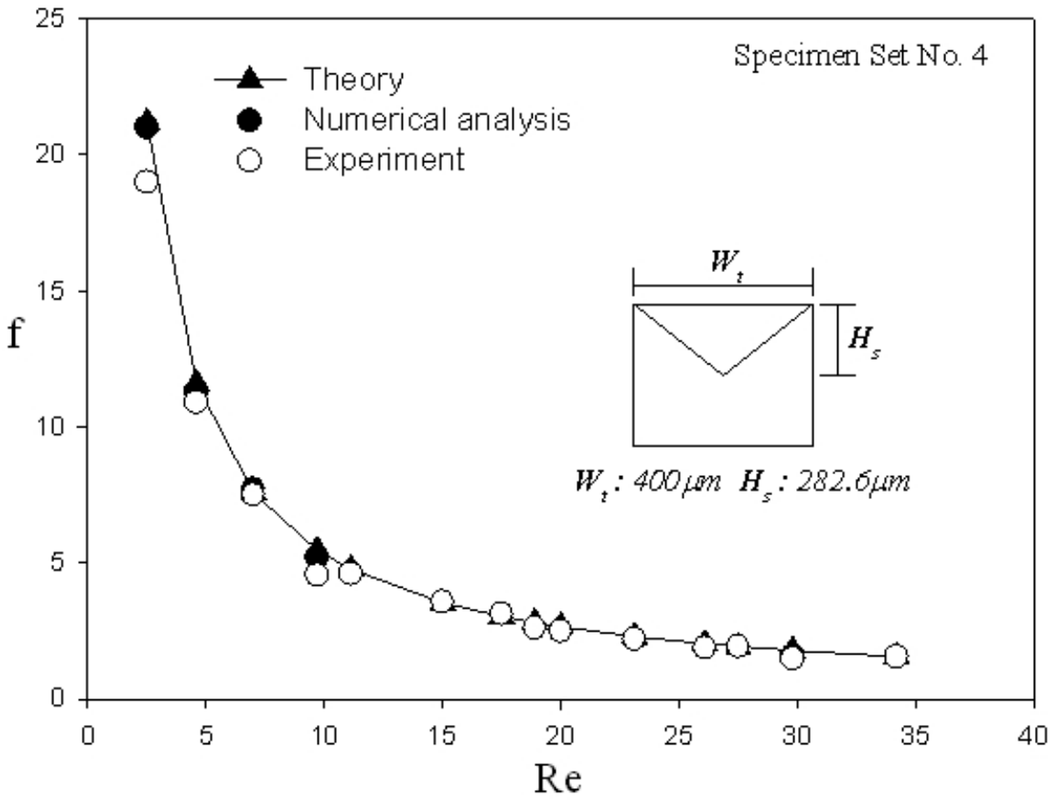

Fig. 3.2. Comparison of f vs. Re for theoretical values, predicted values, and experimental data for Specimen Set No. 4 [3].

Wu and Cheng [29] proposed a correlation for the V-shaped microchannels ($W_b/W_t = 0$) for fluid at low Reynolds numbers as follows.

$$Nu = 6.7\,\mathrm{Re}^{0.946}\,\mathrm{Pr}^{0.488}\left(1-\frac{W_b}{W_t}\right)^{3.547}\left(\frac{W_t}{H}\right)^{3.577}\left(\frac{\varepsilon}{D_h}\right)^{0.041}\left(\frac{D_h}{L}\right)^{1.369}, \mathrm{Re} < 100 \tag{3-2}$$

where W_b and W_t are the bottom and the top width of microchannel, respectively. And ε is the surface roughness.

Referring Wu and Cheng [29], Chu [3] proposed an empirical correlation, based on experimentally obtained data from four sets of triangular microchannel test specimens (with different channel widths) under low Reynolds number conditions (Re < 50).

$$\mathrm{Nu} = \frac{1}{1.2 + (-23.1 + 25.4\mathrm{W_t^{0.5}})^2 \mathrm{Re}^{-2}} \tag{3-3}$$

Generally speaking, the trends of the predicted results obtained from the correlation specified by Eq. (3-3) are in agreement, as shown in Fig. 3.3, while the widths of the microchannels have an obvious impact on the behavior of the development of the Nusselt numbers for the microchannels under study. It is noted that the magnitude of the Nusselt number increases at a slower rate as the Reynolds number becomes larger than 20.

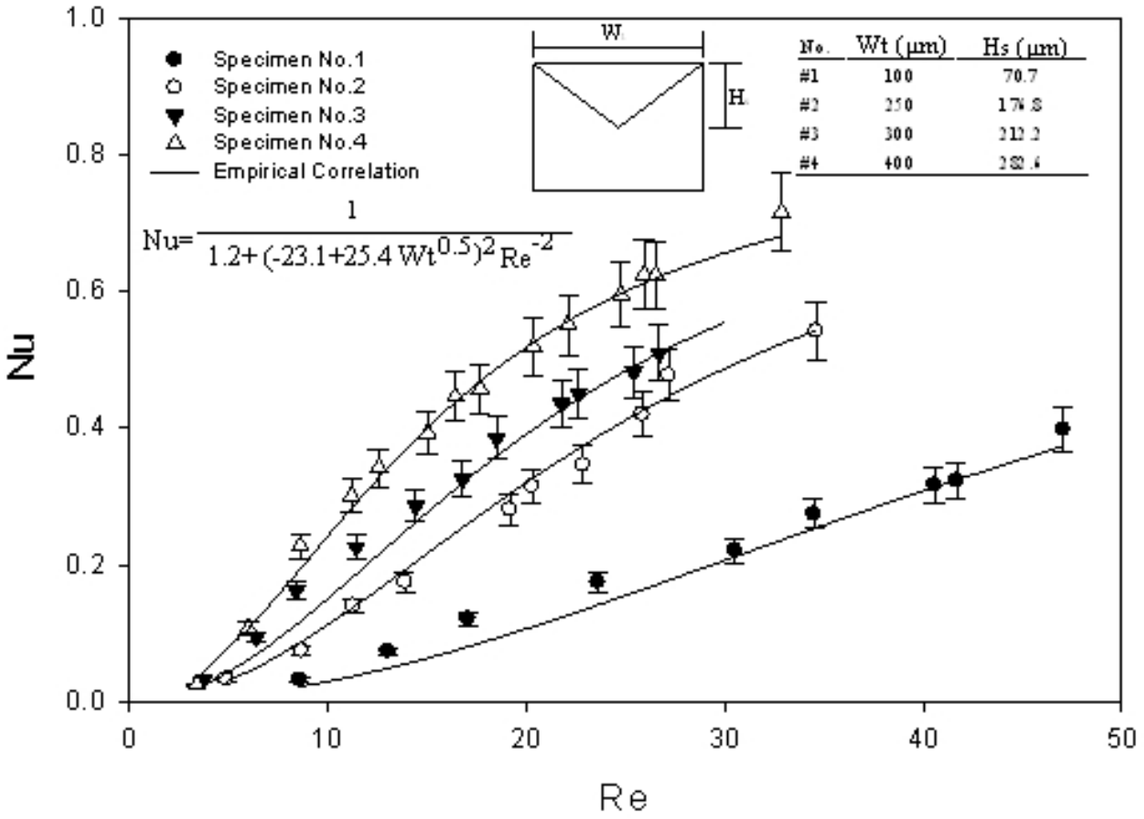

Fig. 3.3. Comparison of Nu vs. Re among empirical correlation and experimental data.

It is also noted that high temperature gradients at the inlet and exit were observed from the temperature distributions of microchannels for all sets of the test specimens. In addition, the Nusselt numbers increase as the Reynolds number increases, as shown in Fig. 3.3.

For the range of the Reynolds number being tested (Re < 50), the average discrepancy of the values calculated from the correlation of Nu obtained in [3] and those obtained from the experimental data is within 15%; the difference is judged to be in fair agreement.

3.2 Flow in circular curved microchannels

Among various micro-fluidic systems such as micro-coolers, micro-biochips, micro-reactors, and micro-fuel cells [3], the curved or bended microchannel (as shown in Fig. 3.5) has been identified as being one of the essential elements for shifting the direction of fluid flow, increasing the length of the path of the fluid flow, enhancing mixing efficiency, and improving heat transfer performance within a confined and compact space [24-26]. Therefore, it is extremely important to acquire a fundamental understanding of the flow behavior of fluid in curved microchannels, since its behavior affects the transport phenomena for the design and process control of micro-fluidic systems.

Up to the present time, there have been numerous investigations in the characteristics of the flow inside straight microchannels. However, a review of the literatures relative to researches conducted in straight microchannels during the last decade [37, 38] has revealed that only a handful of experimental or computational evaluations were done on the study of flow characteristics in curved microchannels [39-41].

For the manufacture of curved microchannels, Chu [3] demonstrated that the curved microchannel could be constructed by standard etching processes; the curved microchannel was etched on a silicon wafer with a 4-inch diameter and a 550 μm thickness. The processes included SiO_2 deposition, photoresist coating, developing, baking, etc. Subsequently, an inductively coupled plasma (ICP) process accounting for the crystal directional characteristics was used to finish the fabrication of the curved microchannel structure (as shown in Figs. 3.4 and 3.5).

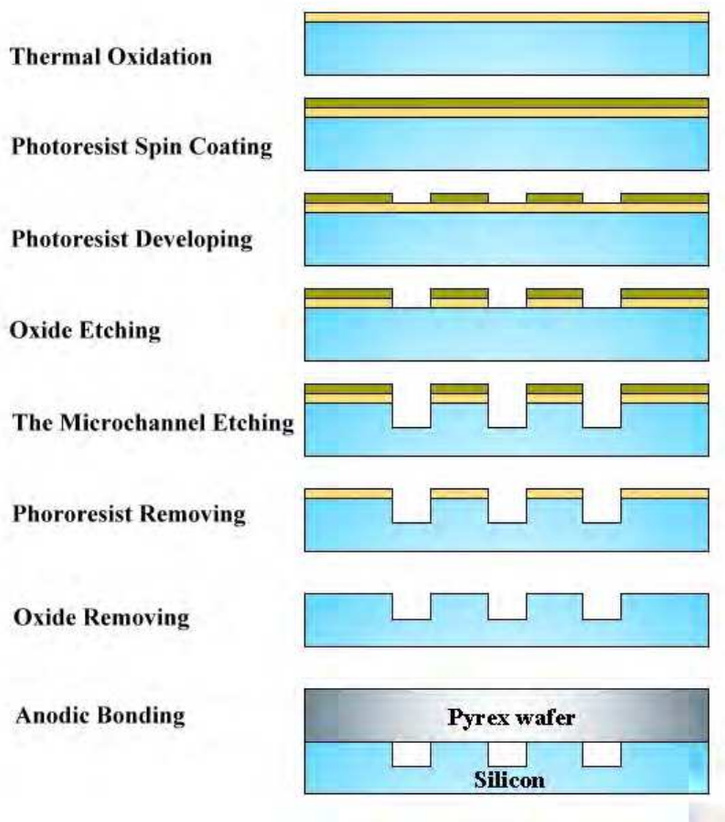

Fig. 3.4. Process flow of fabrication for curved rectangular microchannels.

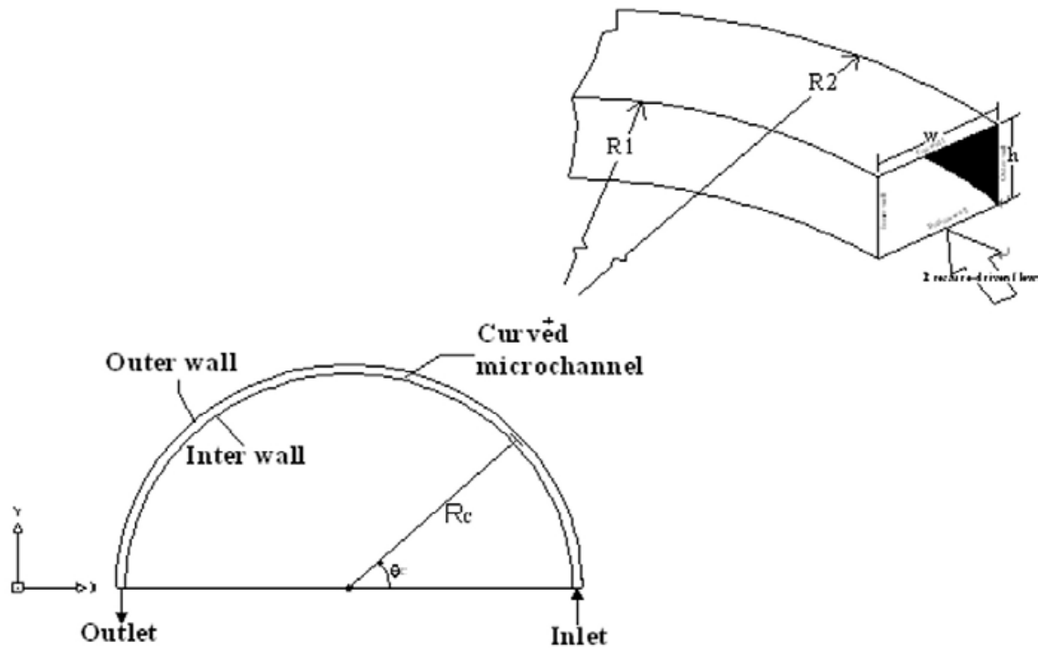

Fig. 3.5. Schematic diagram of the geometry for the curved rectangular microchannel.

For curved microchannels, the geometrical configurations used for testing are given in Table 3.1 [3].

Channel type	Channel width, w (μm)	Channel height, h (μm)	Radius of curvature, R_c (μm)	Aspect ratio, α_c	Curvature ratio
C1	200	200	5,000	1	0.04
C2	200	200	10,000	1	0.02
C3	300	200	5,000	0.667	0.048
C4	300	200	7,500	0.667	0.032
C5	300	200	10,000	0.667	0.024
C6	400	200	5,000	0.5	0.0533
C7	400	200	7,500	0.5	0.0355
C8	400	200	10,000	0.5	0.0266
C9	200	40	5,000	0.2	0.0133
C10	200	40	7,500	0.2	0.0088
C11	200	40	10,000	0.2	0.0066
C12	300	40	7,500	0.133	0.0094
C13	300	40	10,000	0.133	0.007
C14	400	40	5,000	0.1	0.0146
C15	400	40	10,000	0.1	0.0072

Table 3.1. Geometrical parameters of the curved microchannels used for testing

For incompressible flow through horizontal channels of constant cross-sectional area, the Fanning friction factor f_c is based on the mass flow rate and the pressure drop ΔP_f, where the latter is due to the friction occurred inside the curved microchannel.

$$f_c = \frac{2\tau_w}{\rho u_m^2} = \frac{D_h \Delta P_f}{2\rho u_m^2 L} = \frac{180}{\pi R_c \theta_c} \times \frac{w^3 h^3 \Delta P_f}{\rho Q^2 (h+w)} \tag{3-4}$$

where τ_w is the wall shear stress, L is the channel length, u_m is the mean flow velocity, Q is the volumetric flow rate of the working fluid, R_c is the radius of curvature, and θ_c is the angle of the microchannel.

According to the recommendations and method described by Holman [42], Chu [3] proposed the expression of uncertainties associated with Re, f and the product fRe for curved microchannels.

$$\frac{U_{Re}}{Re} = \left[\left(\frac{\delta\rho}{\rho} \right)^2 + \left(\frac{\delta\mu}{\mu} \right)^2 + \left(\frac{\delta Q}{Q} \right)^2 + \left(\frac{\delta h + \delta w}{h + w} \right)^2 \right]^{1/2} \tag{3-5}$$

$$\frac{U_f}{f} = \left[\left(\frac{\delta\rho}{\rho} \right)^2 + \left(\frac{\delta\Delta p}{\Delta p} \right)^2 + 4\left(\frac{\delta Q}{Q} \right)^2 + \left(\frac{\delta L}{L} \right)^2 + 9\left(\frac{\delta h}{h} \right)^2 + 9\left(\frac{\delta w}{w} \right)^2 + \left(\frac{\delta h + \delta w}{h + w} \right)^2 \right]^{1/2} \tag{3-6}$$

$$\frac{U_{fRe}}{fRe} = \left[\left(\frac{\delta\mu}{\mu} \right)^2 + \left(\frac{\delta\Delta p}{\Delta p} \right)^2 + \left(\frac{\delta Q}{Q} \right)^2 + \left(\frac{\delta L}{L} \right)^2 + 9\left(\frac{\delta h}{h} \right)^2 + 9\left(\frac{\delta w}{w} \right)^2 + 4\left(\frac{\delta h + \delta w}{h + w} \right)^2 \right]^{1/2} \tag{3-7}$$

In Eqs. (3-5) – (3-7), it is observed that the measurement errors in the height h and width w of the microchannel dimensions have a significant influence on the overall uncertainty.

In order to compare the flow characteristics of the curved microchannel with those of the conventional dimensions, the relationship between the friction factor and the Reynolds number estimated from the empirical correlation proposed by Yang et al. [43] are plotted in Figs. 3.6 and 3.7 (it should be noted that the correlation was originally proposed by Hua and Yang [44]). The correlation is expressed by the following equation.

$$f = \frac{5}{Re^{0.65}} \left(\frac{w}{2R_c} \right)^{0.175} \tag{3-8}$$

From Figs. 3.6 and 3.7, it is observed that when Re<600, all experimentally-determined friction factors decrease nonlinearly with an increase of the Reynolds number. For the curved microchannels with aspect ratios varying from 0.5 to 1, it was observed that the friction factor of the curved microchannels was mainly affected by the curvature ratio and the Reynolds number. However, for curved microchannels with aspect ratios varying from 0.1 to 0.2, the aspect ratio had a significant effect on the relationship between the friction factor and the Reynolds number.

Another important parameter used to describe the laminar flow fluid behavior in channels is the Poiseuille number Po, which is a product of the friction factor and the Reynolds number. According to the numerical investigation presented by Wang and Liu [45] for a curved microchannel with an aspect ratio of 1 and a curvature ratio of 5×10^{-6}, the predicted relationship between the friction factor ratio and De number, defined by $De = (\rho u_m D_h/\mu)(D_h/2R_c)^{1/2}$, can be expressed by the following equation.

$$fRe_c \,/\, fRe_s = 0.96194 + 0.01035De^{0.78715}, \quad \text{where } 0 < De \leqq 450 \tag{3-9}$$

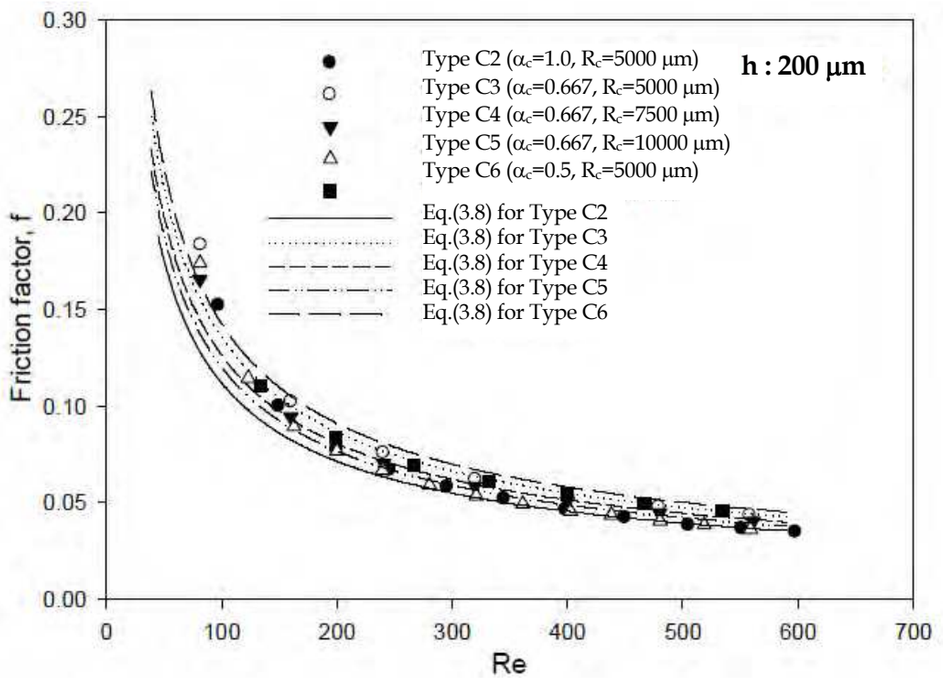

Fig. 3.6. Comparison of friction factor versus Re number for Type C2 to C6 microchannels.

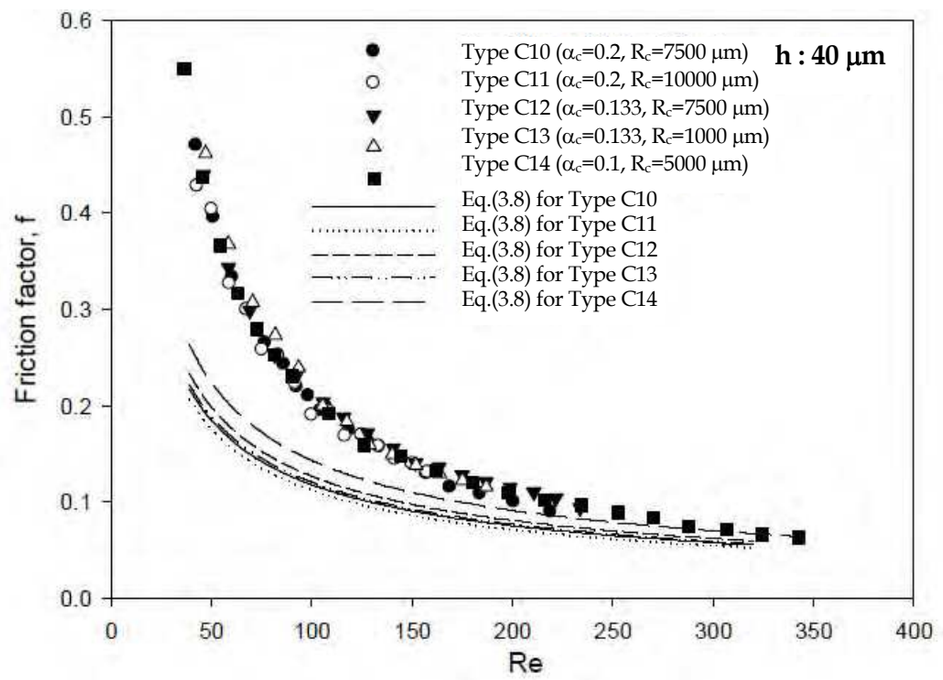

Fig. 3.7. Comparison of friction factor versus Re number for Type C10 to C14 microchannels.

3.3 Flow in fractal-like microchannels

Since the paper published by Tuckerman and Pease [46], manifold microchannel heat sinks using single-phase fluid as coolant have emerged as one of the effective and promising cooling techniques for microelectronic cooling for the last two decades. Due to the high surface-to-volume ratio and compactness for the microchannels, application of microchannels possesses the potential to be an attractive method for cooling micro-system devices. For this reason, numerous investigations have been devoted to fluid flow and heat transfer characteristics of forced convection of water in parallel microchannels [47, 48, 49, 50, 51, 52], and the majority of investigations mainly focused on single phase flow and heat transfer in circular, trapezoidal, rectangular, and parallel plate microchannels by analyzing the variations in the physical behaviors associated with the friction factor, region of transition, and the Nusselt numbers [53]. Moreover, among the extensive studies of micro-thermo-fluidics in straight microchannels, discrepancies were found among the results obtained from the experimental data and those obtained from the classical theories.

Generally speaking, the conventional design of flow architectures such as parallel plate microchannels is based on a unique length scale that is distributed uniformly throughout the available space. However, a network of straight microchannels could cause non-uniform temperature distribution [54, 55], high pressure gradient [56, 57, 58], and flow mal-distribution [59, 60, 61, 62] in the micro-fluidic systems. Thus, it is necessary to develop new type of microchannel geometries to improve the hydrodynamic characteristics of straight microchannel networks.

Consequently, many researchers [63-71] have tried to obtain useful guidelines from the efficient transport properties of nature systems for the design of flow architectures in micro-system.

3.3.1 Model description

Flow architectures are ubiquitous in nature systems such as mammalian circulatory and respiratory networks, arteries and veins in animals, stems and leaves in plants, and river basins [72]. The structure of mammalian lungs is a typical example of a distribution system with a nearly tree-shaped structure.

Bejan and Errera [73] first investigated the architecture of the volume-to-point path such that the flow resistance is minimal. They found that fractal-like networks configuration could provide a minimal flow resistance. Later, Lorente et al. [74] proposed a simpler and direct route to determine the construction of effective fractal-like flow structure in thermal and fluidic systems and discussed the importance of the simplified design method.

To generate a fractal-like microchannel network, the analytical configuration of fractal-like microchannel is characterized by the following constant ratios of the length and hydraulic diameter of the channel at the (k+1)th branching level to the length and hydraulic diameter of the channel at the kth branching level, respectively. The ratios γ and β are defined as:

$$\gamma = \frac{L_{k+1}}{L_k} = N^{-1/D_L} \tag{3-10}$$

$$\beta = \frac{D_{k+1}}{D_k} = N^{-1/D_d} \tag{3-11}$$

where N represents the number of branches into which a single channel is bifurcated, D_L and D_d are fractal dimensions associated with the length and diameter of the channels, respectively, and L_k and D_k represent the length and hydraulic diameter of the fractal-like channel section at branching k, respectively, with k originated from zero.
An initial channel of length L_0 and diameter D_0 bifurcates at one end, and the new channels of length L_1 and diameter D_1 bifurcate at each end to produce the first branching level of the fractal networks, as shown in Fig. 3.8. The bifurcations at the ends of the newly formed channels may be reproduced until the required branching level of the fractal-like microchannel networks is obtained, as shown in Fig. 3.9.

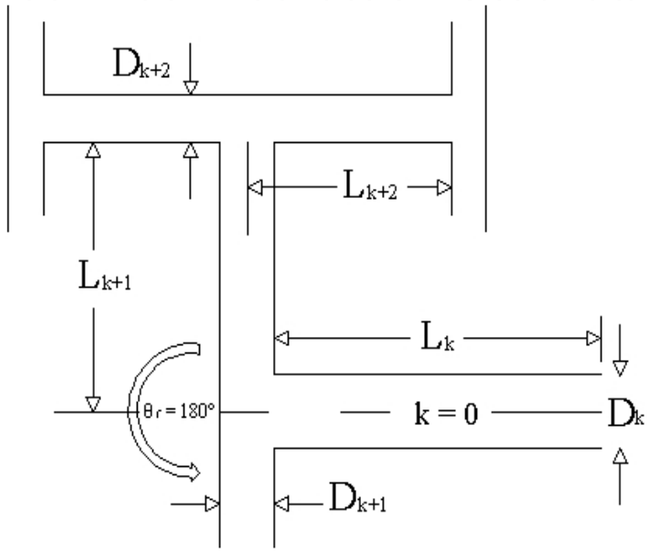

Fig. 3.8. Generation of a fractal-like microchannel networks.

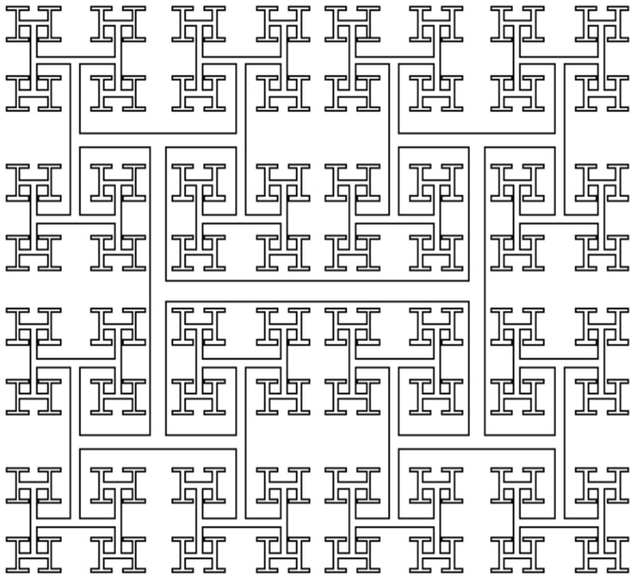

Fig. 3.9. Schematic of the geometric structure of fractal-like microchannel networks with 180° branch angle.

According to Murray's study [75] on cardiovascular system, it has been found that there is an optimal dimension associated with the hydraulic diameter D_d for the fractal-like networks, such that the global flow resistance is minimized. In the study done by Chu [3], the choice of D_d = 3 was taken in the numerical calculations by following the Murray's study, and the values of D_L was taken as 1.4 in setting up the computation domain of fractal-like microchannel networks. In addition, the branching angle θ_f was chosen to be 180°, N was set to be equal to two for the present analysis, and a rectangular cross-section with fixed channel depth was assumed for all of channel branches. The detail dimensions of the fractal-like microchannel networks based on Eqs. (3-10) and (3-11) are given in Table 3.2.

k	0	1	2	3	4	5
H_k (mm)	0.5	0.5	0.5	0.5	0.5	0.5
W_k (mm)	1.5	0.74	0.45	0.30	0.21	0.15
D_k (mm)	0.75	0.60	0.47	0.37	0.30	0.24
L_k (mm)	15	9.14	5.57	3.40	2.07	1.26

Table 3.2. Channel dimensions of the fractal-like microchannel networks

Furthermore, the pumping power in the fractal and parallel channel networks is compared with the theoretical correlation based on the recommendation proposed by Chen and Cheng [53] as follows.

$$P_f/P_p = \frac{[1-(\gamma/(N\beta^4))^{m+1}](1-N\gamma)}{[1-\gamma/(N\beta^4)][1-(N\gamma)^{m+1}]} \tag{3-12}$$

where P_f is the pumping power in fractal-like channel networks and P_p is the pumping power in parallel channel networks.

3.3.2 Results and discussion

The flow in straight microchannels with low Reynolds number is mainly regarded as laminar flow, with a parabolic profile under fully-developed flow condition. However, due to the disturbance effect of channel pattern for the fractal-like microchannel networks, the water flow in straight channel deviates from the laminar situation when the fluid flows through the T-shaped bifurcations. Fig. 3.11 displays the pressure drop variation along Path $A_{a\text{-}b\text{-}c}$ and Path $C_{d\text{-}e\text{-}f}$, and in the middle of the channel (Path B). The measured path of pressure distribution of the fractal-like microchannel networks is shown in Fig. 3.10.

As the water flows through, the sharp increase of pressure is developed in the center and outer sides of the channel, and the inner pressure is rapidly decreasing behind the sharp corner. Then, behind the branches of these T-shaped bifurcations, the distribution of outer and center pressures are dropping immediately, and the velocity boundary layer redevelopment is observed before the next T-shaped bifurcation, as shown in Fig. 3.10. Due to the curvature of the bifurcation, the water flow is directed into a new direction. At this time, the centrifugal forces push the water flow from the center of the inlet channel to the outer wall, and the pressure on the outer side of the channel is increased.

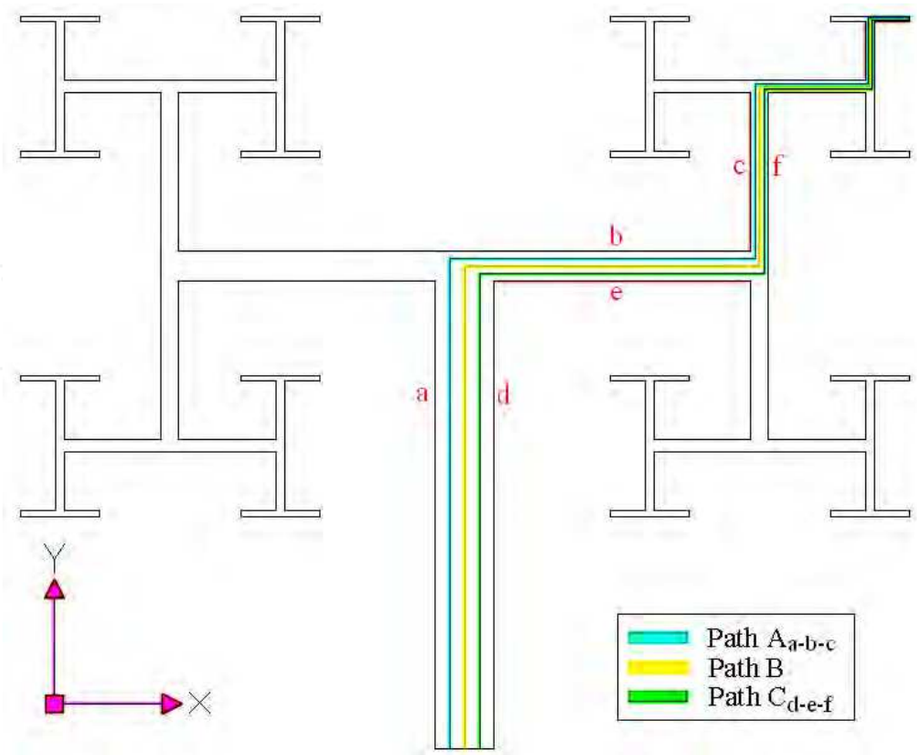

Fig. 3.10. Paths A, B, C (includes branches k=0, k=1, k=2, k=3, k=4, and k=5) and positions of outer and inner walls.

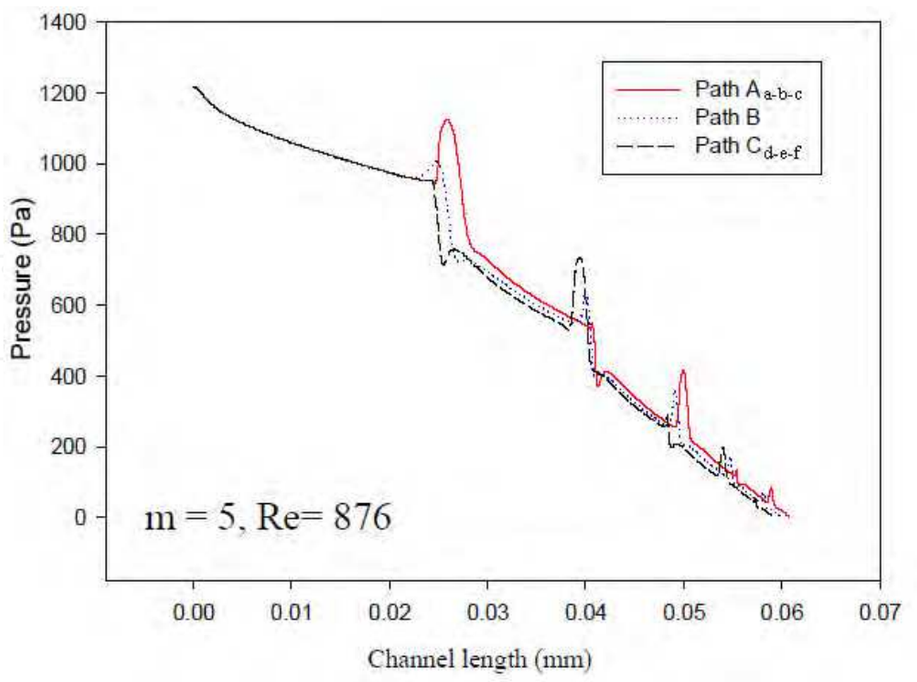

Fig. 3.11. Pressure distribution in fractal-like channel for m=5 case.

In the fractal-like microchannel networks, as the water flow passes through the T-shaped bifurcation, a symmetric double vortex is generated near the top and bottom walls with respect to the centerline of the cross-section as shown in Fig. 3.12. Note that the outside wall is to the right of each flow pattern shown in the Fig. 3.12.

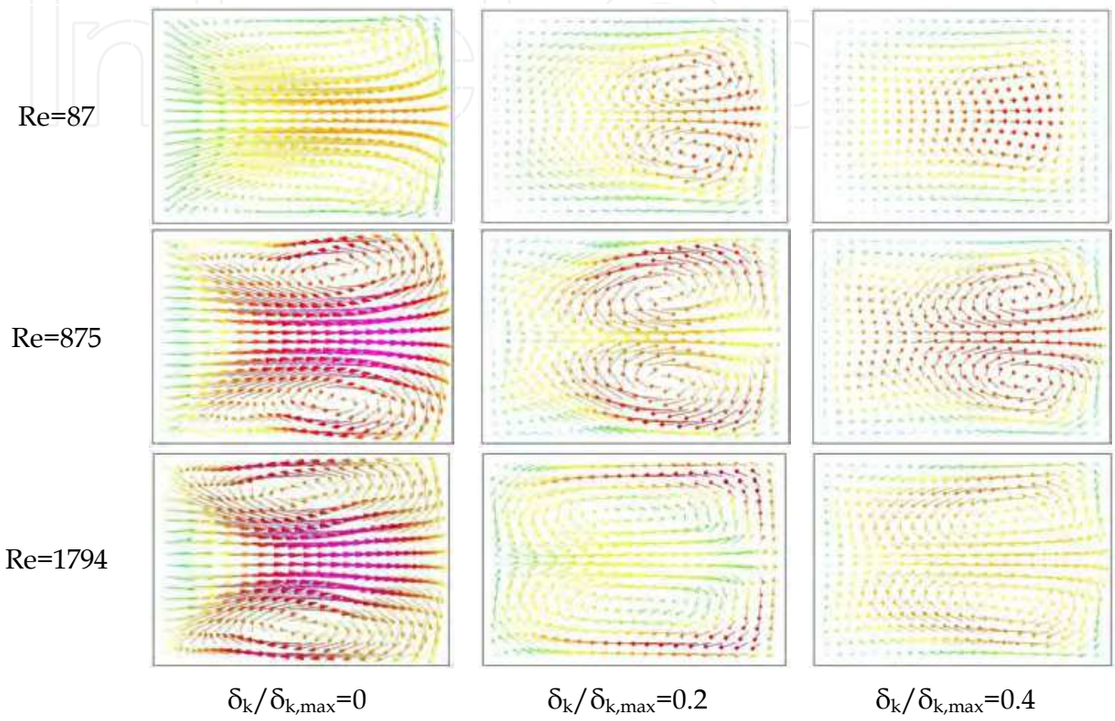

Fig. 3.12. Secondary flow pattern at cross-sections of channels at branch k = 1 with three different Re numbers (which δ_k is the local coordinate indicating the distance from the inlet of the kth bifurcation).

As observed in Fig. 3.12, the secondary flow is composed of two-vortex flow and the type of two-vortex flow rotates in the opposite direction. The flow direction on the centerline is toward the outside wall. As the inlet Reynolds number increases from the k = 1 segment region, the spanwise component of velocity is stronger and the larger secondary velocities are concentrated near the outside wall. However, it can be seen that the secondary flow initiated at the inlet of the branch (k=1) gradually diminishes with increasing distance from the inlet of the branch (k=1).

The variation of pumping power ratios versus the Reynolds numbers at different branching levels is plotted in Fig. 3.13. It is seen that the ratio of pumping powers for the cases with m = 3 to 5 varies linearly as Reynolds number increases, and the variation of pumping powers ratio versus Reynolds number diminishes gradually with increasing branching levels. The region under the P_f/P_p = 1 line indicates that the fractal-like microchannel network exhibits better hydrodynamic performance relative to that of the parallel channel network.

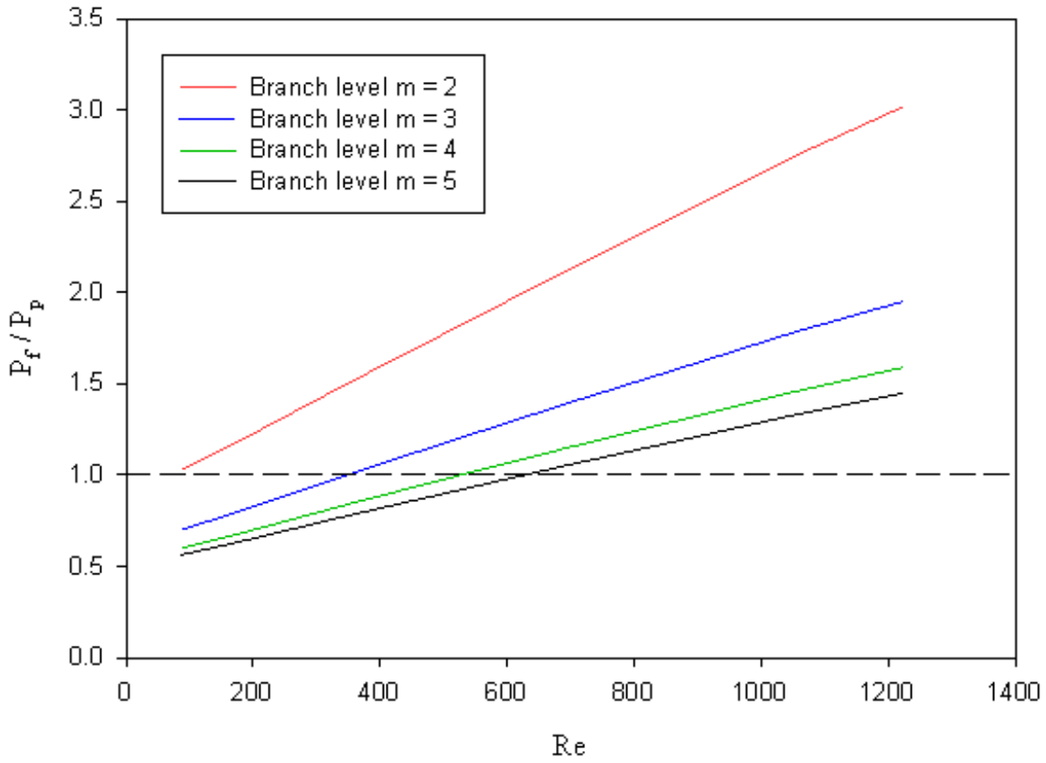

Fig. 3.13. Variation of P_f/P_P versus Re with different branch levels.

4. Flow motion and heat transfer in microchannels with turbulence generators

An experimental study [76] was conducted on the rectangular microchannels with longitudinal vortex generators (LVGs) in the Reynolds number up to 1,200 by using DI water as working fluid. The results can be summarized by three concluding remarks: 1) heat transfer was enhanced with the help of longitudinal vortices in rectangular microchannel while encountering larger pressure drop; 2) it was also found that laminar-to-turbulent transition occurred earlier in rectangular microchannel with LVGs than that for the smooth rectangular microchannel; 3) different configurations of LVGs in rectangular microchannel resulted in different overall heat transfer performance (the ratio of heat transfer enhancement to pressure drop increase), which increased with an increase of the Reynolds number. Discussed below were results of the research studies done by Chu [3] and Liu et al. [76].

4.1 Model description

Dimensions of rectangular microchannels with longitudinal vortex generators are shown in Fig. 4.1. *H*, *W* and *L* are the height, width, and length of microchannels, respectively. The geometrical configuration of LVGs is also shown in Fig. 4.1, which illustrates the length, width, and angle of attack for the LVGs. More details about the locations of LVGs (channel types G1～G7) in test chips are shown in Table 4.1.

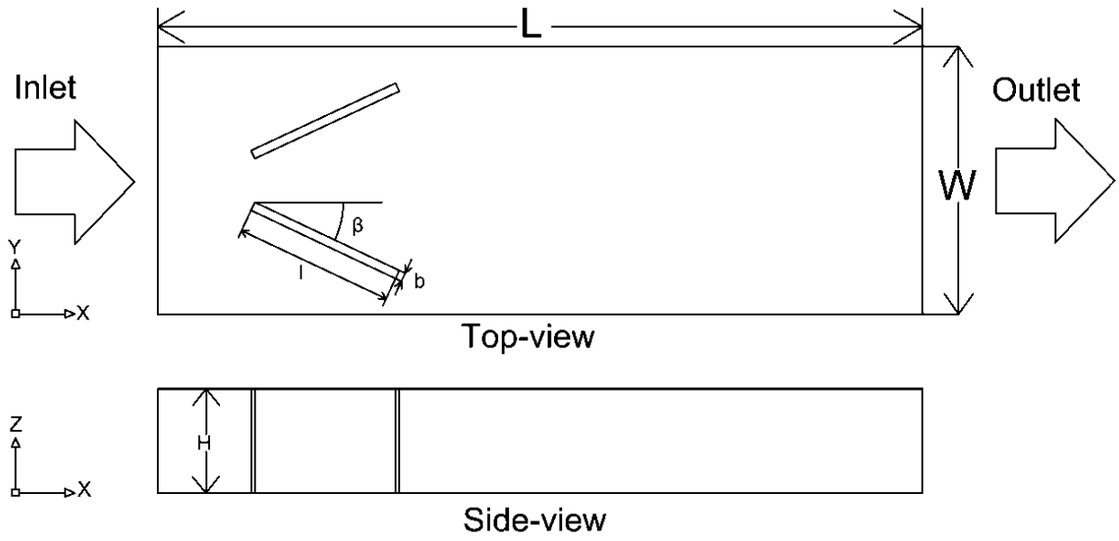

Fig. 4.1. Schematic diagram of rectangular microchannel with longitudinal vortex generators [3, 76].

Channel	Configurations	Schematic Diagram
G1	(5 × 30) or (5 × 150)	
G2	(5 × 45°) or (5 × 135°)	
G3	Smooth channel	
G4	(3 × 30°) or (3 × 150°)	
G6	(30°, 150°, 30°) or (150°, 30°, 150°)	
G7	(45°, 135°, 45°) or (135°, 45°, 135°)	

Table 4.1. List of rectangular microchannel configurations

4.2 Results and discussion

From Fig. 4.2, it can be observed that the rectangular microchannels with LVGs clearly have better heat transfer enhancement than the smooth rectangular microchannel (channel type G4). It can also be seen from Fig. 4.2 that for the rectangular microchannels with LVGs, the slopes of the Nusselt number curves change abruptly when the Reynolds number reaches the range of 600-730. From the conclusion of reference [54], the laminar-to-turbulent transition occurs in a similar range of the Reynolds numbers.

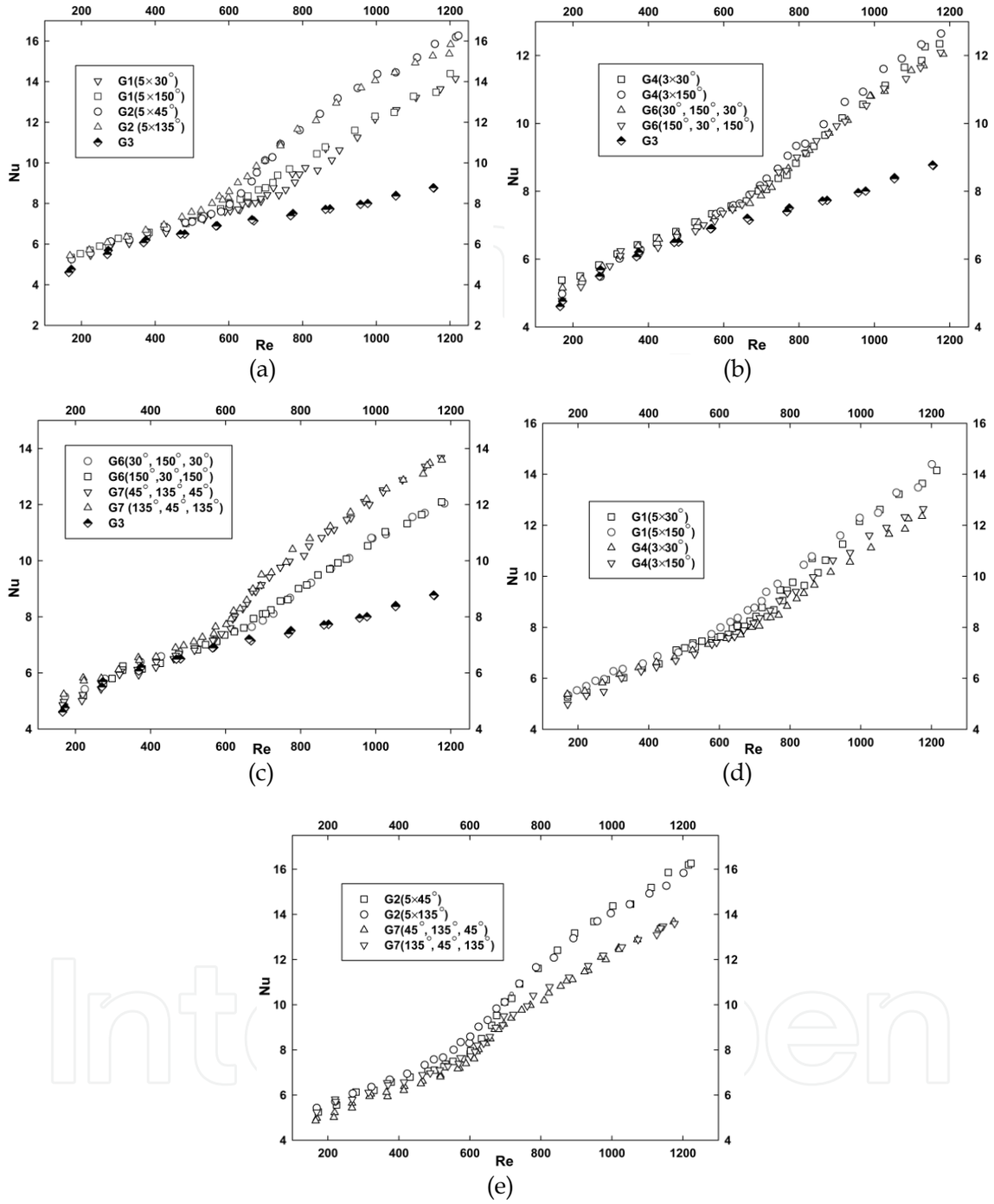

Fig. 4.2. Nusselt number as a function of Reynolds number for microchannels with longitudinal vortex generators [3, 76].

From Fig. 4.3, one can observe that the rectangular microchannels with LVGs result in much larger pressure drop than that for the smooth rectangular microchannel. In addition, different configurations of LVGs in rectangular microchannel demonstrate different fluid flow characteristics.

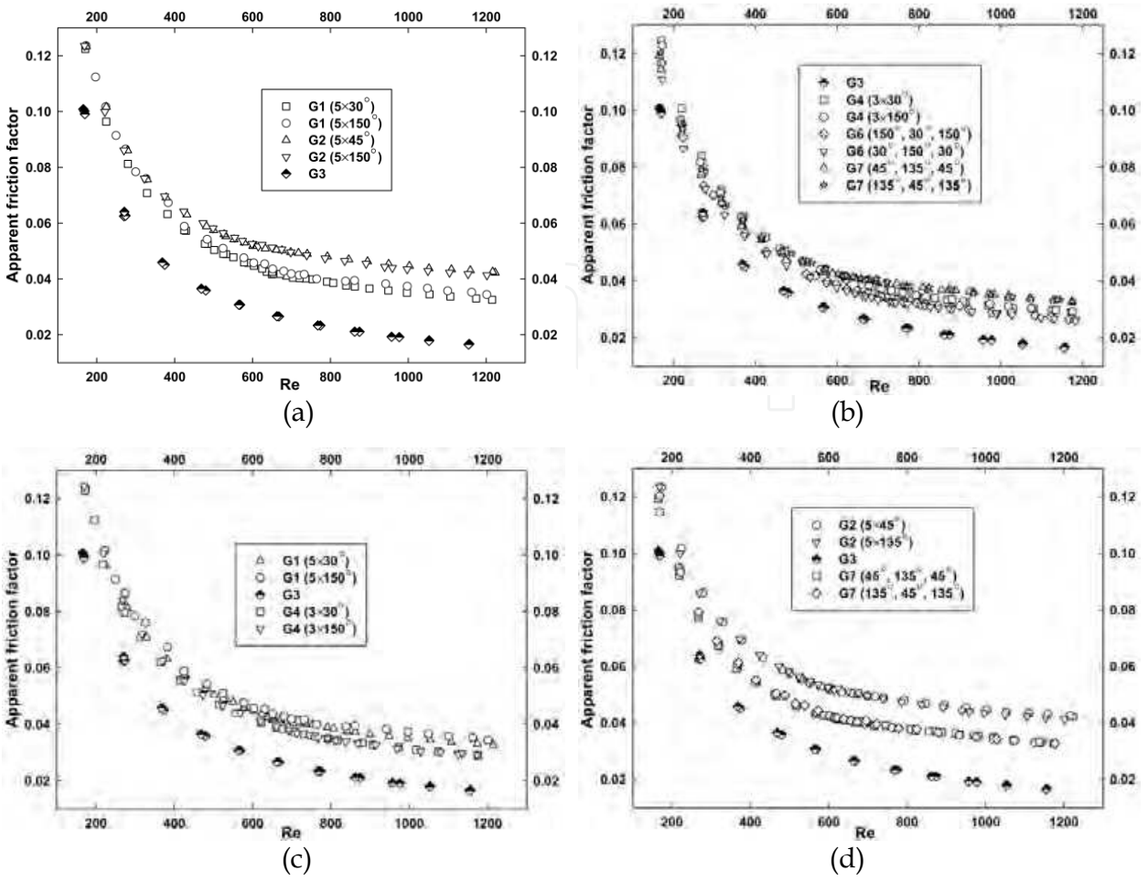

Fig. 4.3. Apparent friction factor as a function of Reynolds number for (a) G1, G2 and G3, (b) G3, G4, G6 and G7, (c) G1, G3 and G4 and (d) G2, G3 and G7 channels [3, 76].

4.3 Empirical correlations

4.3.1 Apparent friction factor correlations

The empirical correlations of experimental data for apparent friction factors are listed in Table 4.2.

	Laminar flow regime	Ranges of applicability	Turbulent flow regime	Ranges of applicability
G1	$f = 7.1 / Re^{0.792}$	$7.8<RePrD_h/L<36$	$f = 0.657 / Re^{0.424}$	$36<RePrD_h/L<61$
G2	$f = 4.657 / Re^{0.707}$	$7.8<RePrD_h/L<31$	$f = 0.324 / Re^{0.286}$	$31<RePrD_h/L<61$
G4	$f=10.016/ Re^{0.859}$	$7.8<RePrD_h/L<36$	$f = 0.875 / Re^{0.482}$	$36<RePrD_h/L<61$
G6	$f = 9.088 / Re^{0.858}$	$7.8<RePrD_h/L<37$	$f = 0.734 / Re^{0.471}$	$37<RePrD_h/L<61$
G7	$f = 7.443 / Re^{0.815}$	$7.8<RePrD_h/L<32$	$f = 0.431 / Re^{0.364}$	$32<RePrD_h/L<61$

Table 4.2. Empirical correlations for apparent friction factors

4.3.2 Heat transfer correlations

For laminar and turbulent flows in rectangular microchannels with LVGs, the empirical correlations (obtained by curve-fitting) of the experimental data are shown in Table 4.3.

Channel	Laminar flow regime	Ranges of applicability
G1	$Nu = 4.76 + \frac{0.366(\mathrm{Re}\,\mathrm{Pr}\,D_h / L)^{1.253}}{1 + 5.56(\mathrm{Re}\,\mathrm{Pr}\,D_h / L)^{0.095}}$	$7.8<RePrD_h/L<36$
G2	$Nu = 4.67 + \frac{0.329(\mathrm{Re}\,\mathrm{Pr}\,D_h / L)^{1.322}}{1 + 4.041(\mathrm{Re}\,\mathrm{Pr}\,D_h / L)^{0.189}}$	$7.8<RePrD_h/L<31$
G4	$Nu = 4.26 + \frac{0.432(\mathrm{Re}\,\mathrm{Pr}\,D_h / L)^{1.358}}{1 + 2.595(\mathrm{Re}\,\mathrm{Pr}\,D_h / L)^{0.471}}$	$7.8<RePrD_h/L<36$
G6	$Nu = 4.07 + \frac{0.418(\mathrm{Re}\,\mathrm{Pr}\,D_h / L)^{1.357}}{1 + 2.321(\mathrm{Re}\,\mathrm{Pr}\,D_h / L)^{0.479}}$	$7.8<RePrD_h/L<37$
G7	$Nu = 4.5 + \frac{0.364(\mathrm{Re}\,\mathrm{Pr}\,D_h / L)^{1.168}}{1 + 5.269(\mathrm{Re}\,\mathrm{Pr}\,D_h / L)^{0.015}}$	$7.8<RePrD_h/L<31$
Channel	**Turbulent flow regime**	**Ranges of applicability**
G1	$Nu = 0.011Re^{0.934}Pr^{1/3}$	$36<RePrD_h/L<61$
G2	$Nu = (19.85 - 372.1Re^{-0.5})Pr^{1/3}$	$31<RePrD_h/L<61$
G4	$Nu = 0.0182Re^{0.845}Pr^{1/3}$	$36<RePrD_h/L<61$
G6	$Nu = 0.0311Re^{0.763}Pr^{1/3}$	$37<RePrD_h/L<61$
G7	$Nu = (39.03 - 221.5/\ln Re)Pr^{1/3}$	$31<RePrD_h/L<61$

Table 4.3. Empirical correlations for Nusselt numbers [3]

5. Concluding remarks

The above topic was chosen to be included in this chapter on Fluid Dynamics in Microchannels due to the fact that one of the key research categories done in Thermo-Fluids Analysis Group (TFAG) Lab at Department of Mechanical Engineering, Chung Yuan Christian University in Chung-Li, Taiwan, is associated with the study on the behaviors of fluid flow and heat transfer for water flowing through microchannels. In addition, fluid flow of micro-scale channels is of interest to many researchers, academicians, and practitioners; thus, the topic was deemed to be an appropriate one to be included in the book on Fluid Dynamics.

This chapter summarized the work performed and the results obtained in both fluid flow and heat transfer done by TFAG over the last several years. The authors would like to express their deep appreciation for the financial supports obtained from National Science Council, Taiwan (Grant Nos. NSC93-2212-E-033-012, NSC94-2212-E-033-017, NSC95-2212-E-033-066, NSC96-2212-E-033-039, NSC97-2212-E-033-050, and NSC99-2212-E-033-025) and Chung Yuan Christian University (Grant No. CYCU-98-CR-ME).

6. Nomenclature

A	Microchannel Area, m^2
A_{ch}	Microchannel Area, m^2
c_p	Specific heat at constant pressure, kJ kg^{-1} K^{-1}
c_v	Specific heat at constant volume, kJ kg^{-1} K^{-1}

D_c	Diameter of microchannel, m
D_d	Fractal dimensions associated with the diameter
De	Dean number
D_h	Hydraulic diameter, m
D_L	Fractal dimensions associated with the length
D_{le}	Laminar equivalent diameter, Eq. (2-11)
Ec	Eckert number
f	Friction factor
G	Vortex generator
H	Microchannel height, m
k	Branch serial number
K	Friction factor for minor loss (Eq. (3-8))
	Hagenbach factor (Eq. (2-8))
L	Microchannel length, m
$\dot{m}$	Mass flow rate, kg s^{-1}
N	Number of branches in fractal-like microchannels
Nu	Nusselt number
P_o	Poiseuille number
Pr	Prandtl number
P_w	Wetted perimeter, m
Q	Volumetric flow rate, m^3 s^{-1}
R_c	Radius of curvature, m
Re	Reynolds number
S	Source term (Eq. (1-1))
T	Temperature, K
u	Velocity, m s^{-1}
W	Microchannel width, m
W_b	Bottom width of trapezoidal microchannels
W_t	Top width of trapezoidal microchannels
ε	Surface roughness, m

Greek symbols

a_c	Aspect ratio
β	Diameter ratio
γ	Length ratio
θ	Angle of vortex generator
λ	thermal conductivity, W m^{-1} K^{-1}
μ	Dynamic viscosity, kg m^{-1} s^{-1}
ρ	Density, kg m^{-3}
τ	Shear stress, N m^{-2}

Subscripts

app	Apparent
c	Contraction
ch	Channel
e	Expansion
h	Hydraulic

i	Inlet
m	Arithmetic mean
o	Outlet
s	Bottom side of microchannel test chip
t	Turbulent

7. References

[1] Frank P. Incropera, David P. Dewitt, Fundamentals of Heat and Mass Transfer, Third edition, Wiley, 1990.

[2] S. G. Kandlikar, S. Garimella, D. Li, S. Colin and M. R. King, Heat Transfer and Fluid Flow in Minichannels and Microchannels, Elsevier Pte Ltd, Singapore, 2006.

[3] J. C. Chu, A Study on the Thermo-Fluidic Behaviors of Water Flowing through Microchannels, Ph.D. Dissertation, Department of Mechanical Engineering, Chung Yuan Christian University, July 2010.

[4] J. P. Van Doormaal and G. D. Raithby, "Enhancements of the SIMPLE method for predicting incompressible fluid flows," Numerical Heat Transfer, Vol.7, No. 2, pp. 147-163, 1984

[5] M. Peric, R. Kessler, and G. Scheuerer, "Comparison of finite-volume numerical methods with staggered and collocated grids," Computers and Fluids, Vol. 16, No. 4, pp. 389-403, 1988.

[6] J. P. Van doormaal and G. D. Raithby, "Enhancements of the SIMPLE method for predicting incompressible fluid flows," Numerical Heat Transfer, Vol. 7, pp. 147-163, 1984.

[7] R. J. Phillips, Forced convection, liquid cooled, microchannel heat sinks, MS Thesis, Department of Mechanical Engineering, Massachusetts Institute of Technology, Cambridge, MA, 1987.

[8] W. M. Kays and A. L. London, Compact Heat Exchangers, New York, NY, McGraw-Hill, pp. 105-112, 1984.

[9] W. L. Qu, G. M. Mala, and D. Q. Li, "Pressure-driven water flows in trapezoidal silicon microchannels," International Journal of Heat and Mass Transfer, Vol. 43, pp. 353-364, 2000.

[10] J. Judy, D. Maynes, and B. W. Webb, "Characterization of frictional pressure drop for liquid flows through microchannels," International Journal of Heat and Mass Transfer, Vol. 45, pp. 3477-3489, 2002.

[11] D. Lelea, S. Nishio, and K. Takano, "The experimental research on microtube heat transfer and fluid flow of distilled water," International Journal of Heat and Mass Transfer, Vol. 47, pp. 2817-2830, 2004.

[12] M. J. Kohl, S. I. Abdel-Khalik, S. M. Jeter, and D. L. Sadowski, "An experimental investigation of microchannel flow with internal pressure measurements," International Journal of Heat and Mass Transfer, Vol. 48, pp. 1518-1533, 2005.

[13] F. F. Abdelall, G. Hahn, S. M. Ghiaasiaan, S. I. Abdel-Khalik, S. S. Jeter, M. Yoda, and D. L. Sadowski, "Pressure drop caused by abrupt flow area changes in small channels," Experimental Thermal and Fluid Science, Vol. 29, pp. 425-434, 2005.

[14] R. K. Shah and A. L. London, Laminar flow forced convection in ducts, Advances in heat transfer supplement, Academic Press, New York, 1978.

[15] F. F. Abdelall, G. Hahn, S. M. Ghiaasiaan, S. I. Abdel-Khalik, S. S. Jeter, M. Yoda, and D. L. Sadowski, "Pressure drop caused by abrupt flow area changes in small channels," Experimental Thermal and Fluid Science, Vol. 29, pp. 425-434, 2005.
[16] P. Hrnjak and X. Tu, "Single phase pressure drop in microchannels," International Journal of Heat and Fluid Flow, Vol. 28, pp. 2-14, 2007.
[17] G. H. Tang, Z. Li, Y. L. He, and W. Q. Tao, "Experimental study of compressibility, roughness and rarefaction influences on microchannel flow," International Journal of Heat and Mass Transfer, Vol. 50, pp. 2282-2295, 2007.
[18] R. J. Phillips, Microchannel heat sinks, Advances in Thermal Modeling of Electronic Components and Systems, New York, NY: Hemisphere Publishing Corporation, 1990, Chapter 3
[19] A. Bucci, G. P. Celata, M. Cumo, E. Serra, and G. Zummo, "Water single-phase fluid flow and heat transfer in capillary tubes," Paper No. ICMM2004-2406, Second International Conference on Microchannels and Minichannels, Rochester, NY USA, pp. 221-228, June 17-19, 2004.
[20] R. Baviere, F. Ayela, S. Le Person, and M. Farve-Marient, "An experiment study of water flow in smooth and rough rectangular microchannels," Paper No.ICMM2004-2338, Second International Conference on Microchannels and Minichannels, Rochester, NY USA, pp. 221-228, June 17-19, 2004.
[21] D. J. Schmitt, and S. G. Kandlikar, "Effects of repeating microstructures on pressure drop in rectangular minichannels," Paper No. ICMM2005-75111, ASME, Third International Conference on Microchannels and Minichannels, Toronto, Canada, June 13-15, 2005.
[22] Z. X. Li, D. X. Du, and Z. Y. Guo, "Experiment study on flow characteristics of liquid in circular microtubes," Proceeding of the International Conference on Heat Transfer and Transport Phenomena in Microscale, Banff, Canada, pp. 162-167, October 15-20, 2000.
[23] R. K. Shah and A. L. London, Laminar flow forced convection in ducts, Advances in heat transfer supplement, Academic Press, New York, 1978.
[24] Pho-Seng Lee, Suresh V. Garimella, and Dong Liu, "Investigation of heat transfer in rectangular microchannels," International Journal of Heat and Mass Transfer, Vol. 48, pp. 1688-1704, 2005.
[25] S. M. Flockhart and R. S. Dhariwal, "Experimental and numerical investigation into the flow characteristics of channels etched in <100> silicon," Journal of Fluids Engineering, Vol. 120, pp. 291-295, 1998.
[26] W. Qu, G. M. Mala, and D. Li, "Heat transfer for water flow in trapezoidal silicon microchannels," International Journal of Heat and Mass Transfer, Vol. 43, pp. 3925-3936, 2000.
[27] W. L. Qu, G. M. Mala, and D. Q. Li, "Pressure-driven water flows in trapezoidal silicon microchannels," International Journal of Heat and Mass Transfer, Vol. 43, pp. 353-364, 2000.
[28] G. Hetsroni, A. Mosyak, Z. Segal, and G. Ziskind, "A uniform temperature heat sink for cooling of electronic devices," International Journal of Heat and Mass Transfer, Vol. 45, pp. 3275-3286, 2002.

[29] H. Y. Wu and P. Cheng, "An experimental study of convective heat transfer in silicon microchannels with different surface conditions," International Journal of Heat and Mass Transfer, Vol. 46, pp. 2547-2556, 2003.
[30] H. Y. Wu and P. Cheng, "Friction factors in smooth trapezoidal silicon microchannels with different aspect ratios," International Journal of Heat and Mass Transfer, Vol. 46, pp. 2519-2525, 2003.
[31] I. Tiselj, G. Hetsroni, B. Mavko, A. Mosyak, E. Pogrebnyak, and Z. Segal, "Effect of axial conduction on the heat transfer," International Journal of Heat and Mass Transfer, Vol. 47, pp. 2551-2565, 2004.
[32] I. Tiselj, G. Hetsroni, B. Mavko, A. Mosyak, E. Pogrebnyak and Z. Segal, "Effect of axial conduction on the heat transfer in microchannels," International Journal of Heat and Mass Transfer, Vol. 47, pp. 2551-2565, 2004.
[33] G. L. Morini, "Viscous heating in liquid flows in microchannels," International Journal of Heat and Mass Transfer, Vol. 48, pp. 3637-3647, 2005.
[34] M. Yi and H. H. Bau, "The kinematics of bend-induced mixing in micro-conduit," International Journal of Heat Fluid Flow, Vol. 24, pp. 645-656, 2003.
[35] N. Kockmann, M. Engler, D. Haller, and P. Wolas, "Fluid Dynamics and Transfer Processes in Bended Microchannels," Heat Transfer Engineering, Vol. 26, pp. 71-78, 2005.
[36] F. Schonfeld and S. Hardt, "Simulation of helical flows in microchannels," AIChE Journal, Vol. 50, pp. 771-778, 2004.
[37] G. L. Morini, "Single-phase convective heat transfer in microchannels: a review of experimental results," International Journal of Thermal Sciences, Vol. 43, pp. 631-651, 2004.
[38] T. Bayraktar and S. B. Pidugu, "Characterization of liquid flows in microfluidic systems," International Journal of Heat and Mass Transfer, Vol. 49, pp. 815-824, 2006.
[39] Y. Yamagucgi, F. Takagi, K. Yamashita, H. Nakanura, H. Maeda, K. Sotowa, K. Kusakabe, Y. Yamasaki, and S. Morooka, "3-D Simulation and visualization of laminar flow in a microchannel with hair-pin curves," AIChE Journal, Vol. 50, pp. 1530-1535, 2004.
[40] W. H. Yang, J. Z. Zhang, and H. E. Cheng, "The study of flow characteristics of curved microchannel," Applied Thermal Engineering, Vol. 25, pp. 1894-1907, 2005.
[41] L. Wang and F. Liu, "Forced convection in slightly curved microchannels," International Journal of Heat and Mass Transfer, Vol. 50, pp. 881- 897, 2007.
[42] J. P. Holman, Experimental Methods for Engineers, McGraw-Hill, New York, 1984.
[43] W. H. Yang, J. Z. Zhang and H. E. Cheng, "The study of flow characteristics of curved microchannel," Applied Thermal Engineering, Vol. 25, pp. 1894-1907, 2005.
[44] S. Z. Hua and X. N. Yang, Actual Fluid Friction Manual, National Defense Industry Press, Beijing, pp. 269, 1985.
[45] L. Wang and F. Liu, "Forced convection in slightly curved microchannels," International Journal of Heat and Mass Transfer, Vol. 50, pp. 881- 897, 2007.
[46] D. B. Tuckermann and R. F. W. Pease, "High performance heat sinking for VLSI," IEEE Electron Device Letters, EDL-2, pp. 126-129, 1981.
[47] W. Qu, G. M. Mala, and D. Li, "Heat transfer for water flow in trapezoidal silicon microchannels," International Journal of Heat and Mass Transfer, Vol. 43, pp. 3925-3936, 2000.

[48] G. Hetsroni, A. Mosyak, Z. Segal, and G. Ziskind, "A uniform temperature heat sink for cooling of electronic devices," International Journal of Heat and Mass Transfer, Vol. 45, pp. 3275-3286, 2002.
[49] H. Y. Wu and P. Cheng, "An experimental study of convective heat transfer in silicon microchannels with different surface conditions," International Journal of Heat and Mass Transfer, Vol. 46, pp. 2547-2556, 2003.
[50] I. Tiselj, G. Hetsroni, B. Mavko, A. Mosyak, E. Pogrebnyak, and Z. Segal, "Effect of axial conduction on the heat transfer," International Journal of Heat and Mass Transfer, Vol. 47, pp. 2551-2565, 2004.
[51] D. Lelea, S. Nishio, and K. Takano, "The experimental research on microtube heat transfer and fluid flow of distilled water," International Journal of Heat and Mass Transfer, Vol. 47, pp. 2817-2830, 2004.
[52] W. Owhaib and B. Palm, "Experimental investigation of single-phase convective heat transfer in circular microchannels," Experimental Thermal and Fluid Science, Vol. 28, pp. 105-110, 2004.
[53] G. L. Morini, "Single-phase convective heat transfer in microchannels: a review of experimental results," International Journal of Thermal Sciences, Vol. 43, pp. 631-651, 2004.
[54] G. Hetsroni, A. Mosyak, Z. Segal, and G. Ziskind, "A uniform temperature heat sink for cooling of electronic devices," International Journal of Heat and Mass Transfer, Vol. 45, pp. 3275-3286, 2002.
[55] I. Tiselj, G. Hetsroni, B. Mavko, A. Mosyak, E.Pogrebnyak and Z. Segal, "Effect of axial conduction on the heat transfer," International Journal of Heat and Mass Transfer, Vol. 47, pp. 2551-2565, 2004.
[56] W. L. Qu, G. M. Mala and D. Q. Li, "Pressure-driven water flows in trapezoidal silicon microchannels," International Journal of Heat and Mass Transfer, Vol. 43, pp. 353-364, 2000.
[57] M. J. Kohl, S. I. Abdel-Khalik, S. M. Jeter, and D. L.Sadowski, "A microfluidic experimental platform with internal pressure measurements," Sensors and Actuators A, Vol. 118, pp. 212-221, 2005.
[58] M. J. Kohl, S. I. Abdel-Khalik, S. M. Jeter, and D. L. Sadowski, "An experimental investigation of microchannel flow with internal pressure measurements," International Journal of Heat and Mass Transfer, Vol. 48, pp. 1518-1533, 2005.
[59] J. M. Commenge, L. Falk, J. P. Corriou, and M. Matlosz, "Optimal design for flow uniformity in microchannel reactors," AIChE Journal, Vol. 48, pp. 345-358, 2002.
[60] E. R. Delsman, A. Pierik, M. H., J. H. De Croon, G. J. Kramer, and J. C. Schouten, "Microchannel plate geometry optimization for even flow distribution at high flow rates," Chemical Engineering Research and Design, Vol. 82, pp. 267-273, 2004.
[61] G. Griffini and A. Gavriilidis, "Effect of microchannel plate design on fluid flow uniformity at low flow rates," Chemical Engineering Technology, Vol. 30, pp.395-406, 2007.
[62] J. T. Teng, J. C. Chu, M. S. Liu, C. C. Wang and R. Greif, "Investigation of the flow maldistribution in microchannels," ASME International Mechanical Engineering Congress (IMECE03), Washington, D.C., November 15-21, 2003.

[63] D. V. Pence, "Reduced pumping power and wall temperature in microchannel heat sinks with fractal-like branching channel networks," Microscale Thermophysical Engineering, Vol. 6, pp. 319-330, 2002.

[64] Y. Chen and P. Cheng, "Heat transfer and pressure drop in fractal tree-like microchannel nets," International Journal of Heat and Mass Transfer, Vol. 45, pp. 2643–2648, 2002.

[65] S. M. Senn and D. Poulikakos, "Laminar mixing, heat transfer and pressure drop in tree-like microchannel nets and their application for thermal management in polymer electrolyte fuel cells," Journal of Power Sources, Vol. 130, pp.178-191, 2004.

[66] A. Y. Alharbi, D. V. Pence, and R. N. Cullion, "Thermal characteristics of microscale fractal-like branching channels," Transactions of the ASME, Vol. 126, pp. 744-752, 2004.

[67] Y. Chen and P. Cheng, "An experimental investigation on the thermal efficiency of fractal tree-like microchannels," International Communications in Heat and Mass Transfer, Vol. 32, pp. 931-938, 2005.

[68] N. Kockmann, M. Engler, D. Haller, and P. Wolas, "Fluid Dynamics and Transfer Processes in Bended Microchannels," Heat Transfer Engineering, Vol. 26, pp. 71-78, 2005.

[69] L. Ghodoossi, "Thermal and hydrodynamic analysis of a fractal microchannel network," Energy Conversion and Management, Vol. 46, pp. 771-788, 2005.

[70] X. Q. Wang, A. S. Mujumdar, and C. Yap, "Thermal characteristics of tree-shaped microchannel nets for cooling of a rectangular heat sink," International Journal of Thermal Sciences, Vol. 45, pp. 1103-1112, 2006.

[71] F. J. Hong, P. Cheng, H. Ge, and G. T. Joo, "Conjugate heat transfer in fractal-shaped microchannel network heat sink for integrated microelectronic cooling application," International Journal of Heat Mass Transfer, Vol. 50, pp. 4986-4998, 2007.

[72] B. Mandelbrot and B. Benoit, The Fractal Geometry of Nature, W. H. Freeman and Company, New York, 1982.

[73] A. Bejan and M. R. Errera, "Deterministic tree networks for fluid flow: geometry for minimal flow resistance between a volume and one point," Fractals, Vol. 5, pp. 685-695, 1997.

[74] S. Lorente, W. Wechsatol, and A. Bejan, "Tree-shaped flow structure designed by minimizing path lengths", International Journal of Heat and Mass Transfer, Vol. 45, pp. 3299-3312, 2002.

[75] C. D. Murray, "The Physiological principle of minimal work in vascular system, and the cost of blood-volume," Proceedings of the National Academy of Sciences, Vol. 12, pp. 207-214, 1926.

[76] C. Liu, J. T.Teng, J. C. Chu, Y. L. Chiu, S. Y. Huang, S. P. Jin, T. T. Dang, R. Greif, and H. H. Pan, "Experimental investigations on liquid flow and heat transfer in rectangular microchannel with longitudinal vortex generators," International Journal of Heat and Mass Transfer, Vol. 54, pp. 3069-3080, 2011.

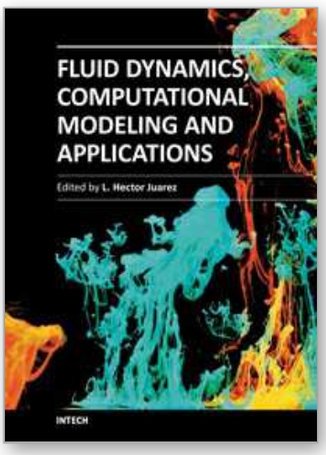

Fluid Dynamics, Computational Modeling and Applications

Edited by Dr. L. Hector Juarez

ISBN 978-953-51-0052-2
Hard cover, 660 pages
Publisher InTech
Published online 24, February, 2012
Published in print edition February, 2012

The content of this book covers several up-to-date topics in fluid dynamics, computational modeling and its applications, and it is intended to serve as a general reference for scientists, engineers, and graduate students. The book is comprised of 30 chapters divided into 5 parts, which include: winds, building and risk prevention; multiphase flow, structures and gases; heat transfer, combustion and energy; medical and biomechanical applications; and other important themes. This book also provides a comprehensive overview of computational fluid dynamics and applications, without excluding experimental and theoretical aspects.

How to reference

In order to correctly reference this scholarly work, feel free to copy and paste the following:

Jyh-tong Teng, Jiann-Cherng Chu, Chao Liu, Tingting Xu, Yih-Fu Lien, Jin-Hung Cheng, Suyi Huang, Shiping Jin, Thanhtrung Dang, Chunping Zhang, Xiangfei Yu, Ming-Tsang Lee, and Ralph Greif (2012). Fluid Dynamics in Microchannels, Fluid Dynamics, Computational Modeling and Applications, Dr. L. Hector Juarez (Ed.), ISBN: 978-953-51-0052-2, InTech, Available from: http://www.intechopen.com/books/fluid-dynamics-computational-modeling-and-applications/fluid-dynamics-in-microchannels

INTECH
open science | open minds

InTech Europe
University Campus STeP Ri
Slavka Krautzeka 83/A
51000 Rijeka, Croatia
Phone: +385 (51) 770 447
Fax: +385 (51) 686 166
www.intechopen.com

InTech China
Unit 405, Office Block, Hotel Equatorial Shanghai
No.65, Yan An Road (West), Shanghai, 200040, China
中国上海市延安西路65号上海国际贵都大饭店办公楼405单元
Phone: +86-21-62489820
Fax: +86-21-62489821

IntechOpen